Theoret. Appl. Mech., Vol. 38, No. 3, pp. 209–297, Belgrade 2011

Recent advances on the measurement and calculation of the elastic moduli of cortical and trabecular bone: a review

Ekaterina Novitskaya[*1], **Po-Yu Chen**[1,2], **Elham Hamed**[3], **Jun Li**[3], **Vlado A. Lubarda**[1], **Iwona Jasiuk**[3], **Joanna McKittrick**[1]

Abstract

In this review, recent advances on the measurement and modeling of elastic properties of cortical and trabecular bone are presented. Bone is a multifunctional material which among its other functions serves as a support for other tissues in the body. As a structural material it is stiff, strong, tough, lightweight and is adaptable. Its excellent mechanical properties are due to its complex, composite and hierarchical structure. In this paper, we outline the experimental approaches that have been used to characterize bone's structure, composition and elastic properties at several different length scales. Then, we discuss different modeling approaches that have been employed to compute bone's elastic moduli. We conclude by discussing the challenges and open issues in this area. Analysis of bone is of importance in orthopedics. Also, gained knowledge on bone can be used by engineers to design new bioinspired composite materials for a wide range of engineering applications.

Keywords: cortical bone, trabecular bone, elastic modulus, modeling, image analysis

[*]Corresponding author, e-mail: eevdokim@ucsd.edu.

[1]University of California, San Diego, Materials Science and Engineering Program, 9500 Gilman Dr., La Jolla, CA 92093.

[2]Department of Materials Science and Engineering, National Tsing Hua University, 101 Sec.2, Kuang-Fu Rd., Hsinchu, Taiwan 30013, R.O.C.

[3]University of Illinois at Urbana-Champaign, Department of Mechanical Science and Engineering, 1206 W.Green St., Urbana, IL 61801.

Contents

1 Introduction

Solid mechanics has traditionally focused on modeling of materials and structures involving synthetic materials such as metals, ceramics, polymers, and composite materials. Natural materials are another class of materials which provide a wide spectrum of possibilities for mechanicians to apply existing theories and experimental techniques and develop new ones. Plants and animals have evolved over billions of years to become very efficient in utilizing materials for their desired functions. Thus, natural, including biological, materials have excellent properties for their applications. Biological materials are often porous, with cellular structures, which gives them light weight and energy-absorbing characteristics as well as high specific stiffness and strength. Such structures are present in trabecular bone and plant stems, for example. Mechanical property map showing Young's elastic modulus as a function of density (Ashby, 1989; Wegst and Ashby, 1994) is shown in Figure 1.1.

Densities of biological materials are low, generally less than 3 g/cm^3; whereas synthetic materials often have densities in the range of 4-15 g/cm^3. There is a broad range in Young's modulus, varying over orders of magnitude. Biological materials are also multifunctional and they adapt to changing environments and often have capacity to heal. Study of natural materials is needed to obtain fundamental understanding of their behavior to address problems in medicine and other fields. We can also look towards nature for ideas so we can adapt them to design superior synthetic materials for a wide range of engineering applications.

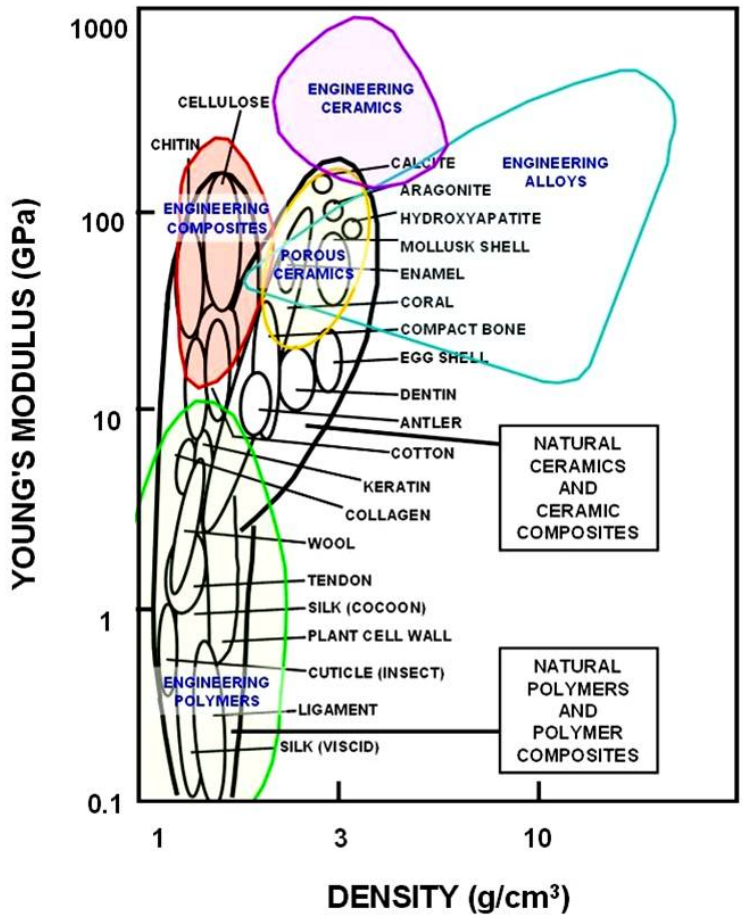

Figure 1.1: Young's modulus as a function of density for biological materials, overlaid on a map indicating regions of synthetic materials. Taken from Ashby (1989) and Wegst and Ashby (1994).

In this paper we address bone, a biological material. Bone is multifunctional: it provides the frame for the body, protects organs, manufactures blood cells, stores useful minerals, maintains pH in the blood, detoxifies, and contributes to movement. As a structural material it is stiff, strong, tough and yet lightweight. In addition, it is continuously adapting to loads and environment by growing larger and thicker when subjected to sufficient loads. Also, it has healing and regenerative characteristics as it heals its microcracks or fractures.

The outstanding mechanical properties of bone are due to its complex composite and hierarchical structure. Bone is composed of three major constituents: an organic matrix (predominately type-I collagen), a mineral reinforcement (calcium phosphate) and water. A small amount of non-collagenous proteins (NCPs) ($\sim 10-15\%$ from the organic matrix (Olszta et al, 2007) that surrounds the minerals and attaches the collagen molecules together is also found. There are two main types of bone: cortical (compact or dense) and trabecular (cancellous or spongy). Cortical bone is the dense bone that forms the outer sheath and it makes up the majority of the skeleton, whereas trabecular bone is sandwiched between cortical bone to give energy absorbent properties (e.g., in skull, ribs, vertebrae) and at ends of long bones (e.g., femoral head) to distribute loads. Mammalian bone is made up of around 65 wt % mineral phase, 25 wt % organic, and 10 wt % water. On a volumetric basis, this corresponds to $\sim$ 33-43 vol % minerals, 32-44 vol % organic, and 15-25 vol % water (Olszta et al., 2007).

There are several books that provide valuable insights into bone. In the 70's, J.D. Currey investigated a broad variety of mineralized biological materials and authored the well-known book *Bones: Structure and Mechanics* (Currey, 2002). Other works of significance are *Skeletal Tissue Mechanics* (Martin, 1998), *Mechanical Testing of Bone and the Bone-Implant Interface* (Ann and Draughn, 1999), *Bone Mechanics Handbook* (Cowin, 2001), and *Tissue Mechanics* (Cowin and Doty, 2007). There have also been a number of overview articles presenting the field in a broad manner. Noteworthy among them are overviews in *Journal of Bone and Joint Surgery* (Reilly, 1974a), *Annual Review of Materials Science* (Weiner, 1998), *Materials Science and Engineering R* (Olszta et al., 2007), and *Osteoporosis International* (Zysset, 2009).

There have been numerous experimental investigations into the evaluation of elastic modulus. Noteworthy are articles by Currey (1969a, 1969b, 1984, 1987, 1988a, 1990, 2010), Bonfield and Datta (1974), Reilly et al. (1974b), Bonfield and Grynpass (1977), Bonfield and Tully (1982), Katz (1980), Evans (1990), and Rho et al. (1993). The main findings are that elastic modulus is dependent on a variety of factors, including:

- type of bone: cortical or trabecular;
  - cortical: osteonal (primary or secondary), interstitial, woven
  - trabecular

- the scale of observation (nano- to macro-);
- taxa of bone (mammal, avian, reptile, etc.);
- skeletal location of the bone (femur, skull);
- amount of mineralization;
- degree of hydration (water content);
- porosity;
- orientation (longitudinal, transverse, radial);
- age;
- strain rate;
- microstructural constituents.

We review recent experimental and theoretical developments and challenges in studies of elastic modulus of bone. Because of the large amount of data and publications on various bone types, we focus here on human and bovine cortical and trabecular femoral bones. The techniques and ideas are generally also applicable to other biological materials. In addition, lessons learned from nature about bone's structure-property relations can give guidance on how to design novel bioinspired synthetic structural materials.

2 Background

2.1 Constituents of bone

2.1.1 Protein structure (collagen)

At the molecular level, three polypeptide chains (two α_1 and one α_2) twist together to form the tropocollagen triple helix molecule that is $\sim$ 280 nm in length and 1.5 nm in diameter, stabilized by numerous hydrogen bonds (Figure 2.1). A defining feature of collagen is the frequently occurring amino acid sequence of Gly-Pro-X or Gly-Y-Hyp (Gly = glycine, Pro = proline, Hyp = hydroxyproline, X, Y = other amino acid residues). Glycine is a majority residue, which is the smallest amino acid and the only one small enough to tuck into the twists along the triple helix. The tropocollagen further self-assembles into fibrils that are $\sim$ 100 nm in diameter and up to several microns in length. The tropocollagen assembles into strands of $\sim$ 300 nm in length and separated by $\sim$ 40 nm. These strands are organized into a staggered array to form collagen fibrils that are 10-200 nm in diameter and are microns to tens of microns long, held together by covalent cross-linked bonds. The interruption between the tropocollagen molecules gives rise to two important dimensions – the gap ($\sim$ 40 nm) and the overlap ($\sim$ 27 nm) regions that combine to

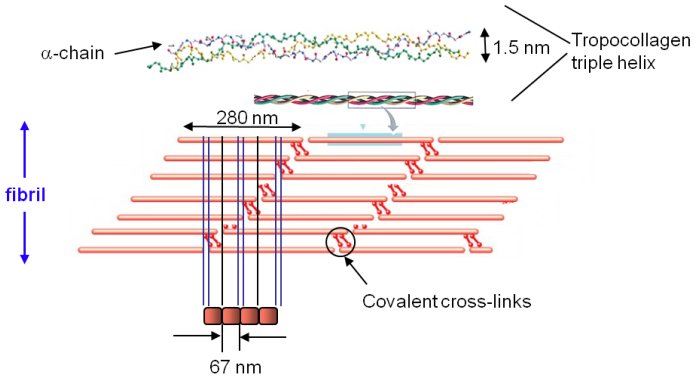

Figure 2.1: Structure of collagen fibrils. Three α-chains twist together to form the tropocollagen molecule. The tropocollagen molecules are held together by covalent bonding and self-assemble to form a fibrous, periodic array consisting of a gap region ($\sim$40 nm) and an overlap region ($\sim$ 27 nm) between the staggered arrays. These staggered arrays form the collagen fibril, 10-200 nm in diameter.

form the characteristic banded structure of 67 nm spacing, observed in transmission electron microscopy (TEM), as shown in Figure 2.2.

2.1.2 Mineral structure (hydroxyapatite)

Bone minerals consist of non-stoichiometric hydroxyapatite crystals (chemical formula, $Ca_5(PO_4)_3OH$, with 4-6% of the phosphate groups replaced by carbonate groups). The bone crystals are in the form of platelets approximately 40-60 nm in length and 20-30 nm in width. The thickness of bone crystals measured by transmission electron microscopy (TEM) (Jackson et al., 1978; Weiner and Price, 1986a; Ziv and Weiner, 1994; Boskey, 2003; Rubin et al., 2003) and small angle X-ray scattering (SAXS) (Fratzl et al., 1992; Watchtel and Weiner, 1994) varies from 1.5 nm for mineralized tendon to 4 nm for some mature bones. Recent atomic force microscopy (AFM) studies found that the bone crystals are longer than those observed by TEM, with widths and lengths ranging from 30 to 200 nm (Tong et al., 2003; Hassenkam et al., 2004). This discrepancy may be due to breakage of the fragile crystallites during TEM sample preparation. Figure 2.3 shows TEM and scanning electron microscopy (SEM) images of bone crystals. In the TEM micrographs, the plate-like structure of the minerals is observed that have dimensions of $\sim$ 20-80 nm in width, and $\sim$ 4 nm in thickness. The SEM image of mineralized collagen fibrils is shown with the bone crystals forming small aggregates of $\sim$ 70

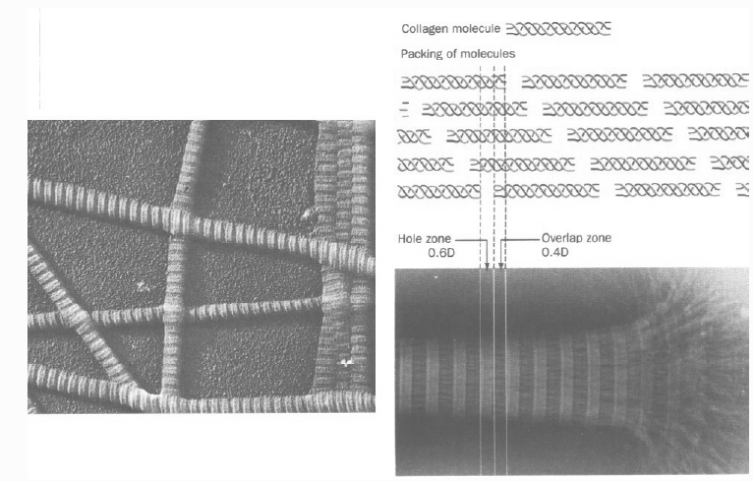

Figure 2.2: Transmission electron microscopy of collagen, showing the characteristic banded pattern arising from the gap and overlap regions. Taken from Voet and Voet (1995).

nm. The mineralized collagen fibril is the basic unit of all bones. Most studies on the structural organization of mineral within collagen fibrils have been carried out on mineralized turkey leg tendon (MTLT) (Berthet-Colominas, 1979; Weiner et al., 1986b; Arsenault, 1991; Erts et al., 1994; Landis et al., 1993, 1996a). TEM observations of individual MTLT showed that mineral crystals are organized in layers that transverse across the fibrils with the crystallographic *c*-axis aligned parallel with the fibril long axis (Berthet-Colominas, 1979; Weiner et al., 1986b; Arsenault, 1991). The 67 nm periodicity of mineralized collagen fibrils shown in TEM indicated that the minerals have the same staggered organization as collagen fibrils. AFM (Erts et al., 1994) and high-voltage three-dimensional (3D) TEM tomography (Landis et al., 1993, 1996b) also confirmed the layered arrangement of crystals within collagen fibrils. However, mineralized turkey leg tendon (mineral content $\sim$ 43 wt %) is not a bone, which has much higher degree of mineralization ($\sim$ 65wt %)and more complicated structure. Figure 2.4 shows the mineralization process in bone. It is generally believed that crystals initially form within the gap region of the collagen fibrils, further proceed into the overlap region, and subsequently grow into the extrafibrillar space (Siperko and Landis, 2001). Consequently, minerals are found both within and outside the collagen fibrils, but the exact amount in each location is still a matter of contention (Katz and Li, 1973; Bonar et al., 1985; Pidaparti et al., 1996; Sasaki et al., 2002; Nikolov and Raabe, 2008). Landis and co-workers proposed a model for early stage mineralization based on the 3D

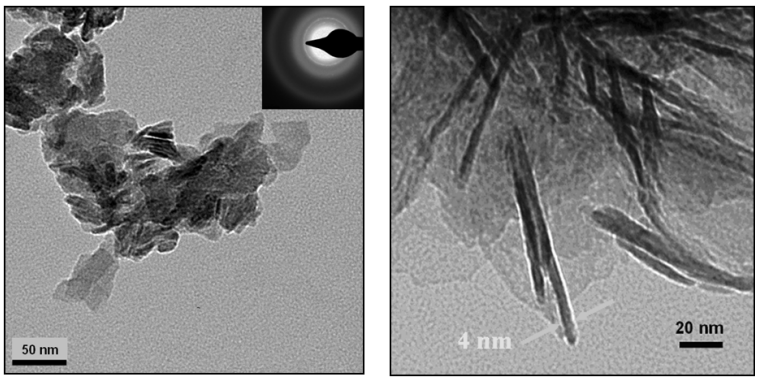

(a)

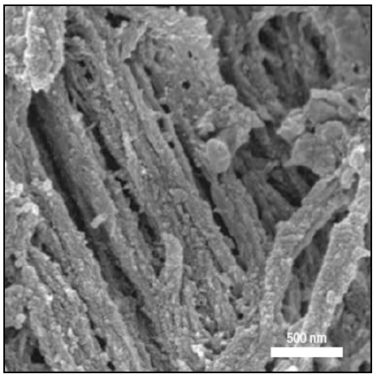

(b)

Figure 2.3: (a) TEM micrographs of the mineral phase (hydroxyapatite) in cortical bovine femur bone. The platelets are $\sim$ 20 x 50 in width and $\sim$ 4 nm in thickness. (b) SEM micrograph of mineralized collagen fibers from human cortical bone. The globules are aggregates of hydroxyapatite. Taken from Fantner et al. (2005)

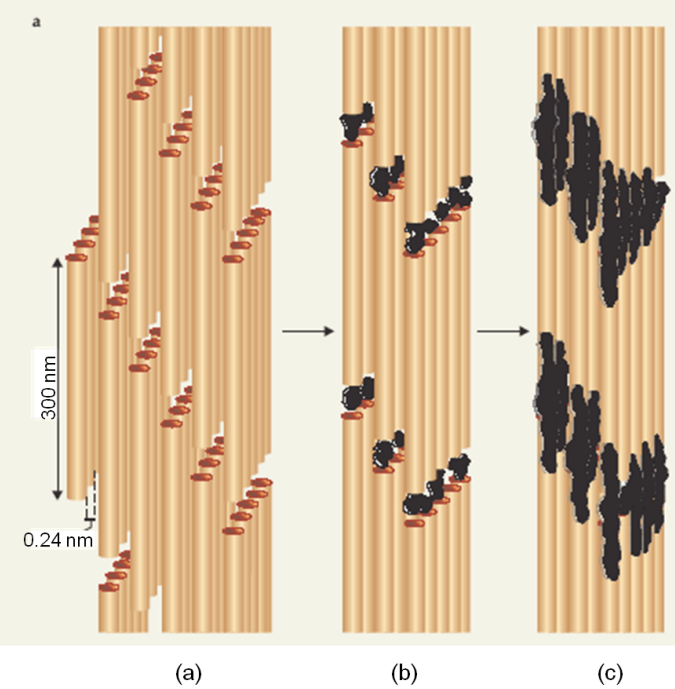

Figure 2.4: Regions where hydroxyapatite is located in the mineralized collagen fibril, either intramolecular or extramolecular: (a) assembly of tropocollagens to form fibrils; (b) nucleation of interfibrillar minerals in the gap region between the tropocollagen molecules; (c) extrafibrillar minerals nucleated outside of the tropocollagen. Taken from Ritchie et al.(2009).

TEM tomography (Landis et al., 1993, 1995, 1996a). The staggered arrangement of collagen fibrils forms extensive channels laterally through the arrays. Mineral crystals develop preferentially in length along the collagen long axes and in width within the spaces generated by the channel. Crystals are fused together and grow in length beyond gap and overlap regions, ranging 40-170 nm and in width to ∼40 nm, well beyond that of individual collagen gap regions. However, the growth in thickness is limited to 4-6 nm. Ultimately, fused mineral crystals form thin parallel sheets throughout the assemblage of collagen fibrils. In the study on mineral crystals in embryonic chick bones, Landis et al. (1996b) have suggested that the mineral sheets may fuse to form a continuous mineral organization.

2.1.3 Water

Water is another significant phase in bone, which plays an important role in the bio-mineralization process and enhancing mechanical properties. Water is located at various hierarchical levels: within the porous regions, such as vascular channels, osteocyte lacunae, and canaliculi, between the lamellae, inside the fibrils (gaps), and surrounding the triple helix tropocollagen molecules (Fullerton and Amurao, 2006; Fullerton et al., 2006; Cameron et al., 2007). Water also plays an important structural role in collagen fibrils. Hydration of the collagen fibril separates adjacent collagen molecules in the lateral plane by a water layer 0.7 nm thick, while not affecting the fibril's axial structure. This lateral fluidity of the fibril allows the precursor constituents that form hydroxyapatite to diffuse within the fibril (Ekani-Nkodo, 2003; Toroian et al., 2007). During mineralization, the water within the fibril is replaced by mineral (Fratzl et al., 1993), causing a loss of the freedom of collagen molecules to move. Water, therefore, helps to define the structural characteristics and physical properties of collagen.

2.2 Hierarchical structure

In biological composites the minerals provide strength and stiffness, while the biopolymers impart toughness. Figure 2.5 shows a Wegst-Ashby map of toughness and elastic modulus for biological materials. The structural biopolymers (e.g. collagen, keratin) show high toughness but low elastic modulus, whereas the minerals have a high elastic modulus but low toughness, given their brittleness. Composites made of biopolymers and minerals, such as teeth and bone, yield materials that result in both the high toughness and elastic modulus, and lightweight. Additionally, the fracture toughness, K_{Ic}, shown as parallel diagonal lines on the diagram, is at the highest level. Thus, these materials are composite materials in their true sense – the combination of dissimilar materials which yields a new material having sought-after properties from each constituent.

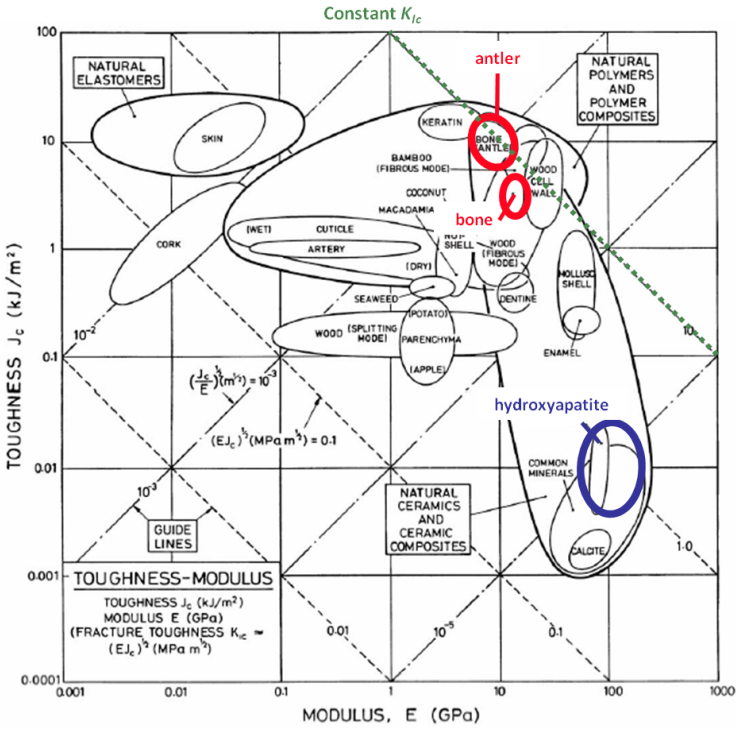

Figure 2.5: Property map of biological materials, showing location of the hydroxyapatite (blue) and bone (red). Modified from Wegst and Ashby (2004).

The hierarchical structure of bone is shown in Figure 2.6. Level I (2-300 nm) has two basic units: the tropocollagen molecule (300 nm length, 1.5 nm diameter) and the mineral, hydroxyapatite (4 nm thickness, 25-100 nm breadth). In Level II (0.1-5 μm), the tropocollagen molecules assemble to form collagen fibrils of $\sim$ 100 nm in diameter. Hydroxyapatite (4 nm thickness, lateral dimension $\sim$25-100 nm), is nucleated within and outside of the fibrils, which are held together by non-collagenous proteins (Fantner, 2005), forming the basic unit of all bone, the mineralized collagen fibril. In Level III (10-50 μm), the fibrils further assemble into oriented arrays of sheet-like structures (lamellae). In these lamellar structures reside lacunae (10-20 μm), which are connected by canaliculi channels (100 nm diameter). Bone cells (osteocytes) reside in lacunae. In Level IV, in cortical bone the lamellae assemble into concentric cylinders, forming the basic unit, the osteon, while in trabecular bone they form flat lamellar rods and struts that enclose a

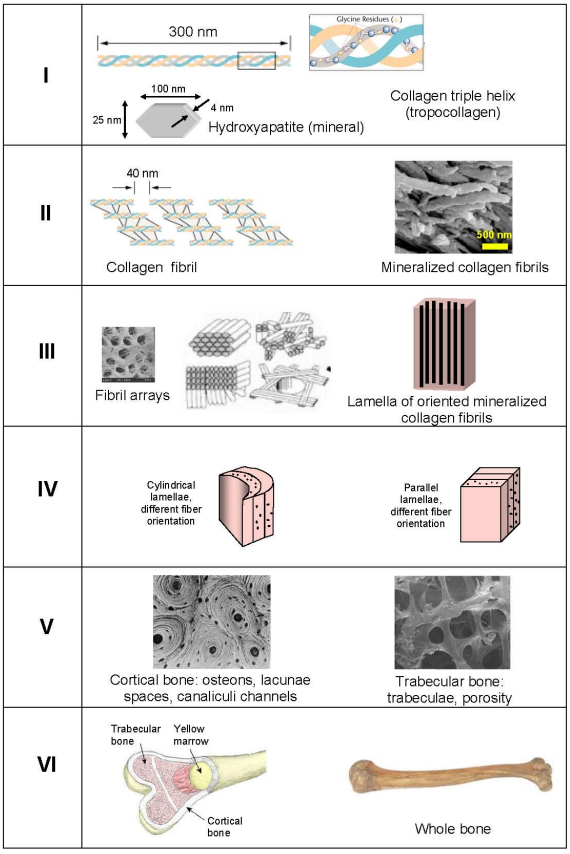

Figure 2.6: Hierarchical structure of bone. Level I: The basic elements of bone, tropocollagen (280 x 1.5 nm) – a triple helix of α-collagen molecules and carbonated hydroxyapatite (platelets of 100 x 25 x 4 nm). Level II: Tropocollagen assembles to form collagen fibrils and combine with hydroxyapatite, which is dispersed between (in the gap regions) and around the collagen, forming mineralized collagen fibrils. Level III: The fibrils are orientated into several structures, depending on the location in the bone (parallel, circumferential, twisted). Level IV: Cortical bone is lamellar – cylindrical and parallel plate lamella is found depending on location. Level V: Optical microscopy image showing osteons (organized cylindrical lamellae) with a central vascular channel and small lacunae (10-20 nm) interspersed between the lamellae, and scanning electron microscopy image of trabecular bone showing a complex trabecular network. Level VI: Whole bone. Taken from Chen et al.(2011).

high level of porosity. Level V represents cortical bone consisting of osteons with a central vascular channel and porous trabecular bone. Level VI is whole bone (a femur).

2.2.1 Importance of porosity

The porosity in bone appears at varying hierarchical levels (Cowin, 1999), as shown in Figure 2.7(a).

At the molecular level, there exists space ($\sim$ 40 nm) between adjacent collagen molecules, where water and NCPs can be found. There are also spaces and gaps between mineralized collagen fibrils, on the order of 1-10 nm. The canaliculi, which are small tubules $\sim$100 nm in diameter, interconnect lacunae spaces in different lamellae and transport nutrient and signals. The elliptically shaped lacunae spaces, where osteocytes reside, are 10-20 μm. The vascular channels, which are filled with blood in the live animal, are 20-50 μm in diameter. Resorption cavities, ranging from 50 μm to 300 μm, can be observed during bone remodeling. Finally, the trabecular bone has pores that range from several hundred micrometers to several millimeters.

Figure 2.7(b) shows a cross-section of cortical bone, displaying more complexity of the vascular system. Volkmann's canals extend perpendicularly to the main vascular channels (Haversian canals), aligned in the bone growth direction. This interconnected vascular network gives rise to oriented, tubular porosity running throughout cortical bone. Additionally cortical bone is surrounded by a periosteal region, which is a tough, strong sheath that protects the interior bone.

3 Structural characterization of bone

Understanding the structure of bone has been challenging due to its hierarchical structure, multiple constituents, and complex porous systems. Here, we review techniques that have been applied to characterize bone. Figure 3.1 summarizes the imaging techniques that can be used to characterize bone at varying hierarchical levels, from nano, micro, to millimeter scales (Lim et al., 2006; Launey et al., 2010).

Each technique has its operating range that is suitable for certain structural features of bone. For example, optical microscopy and X-ray computed tomography (CT) are typically used for observing bone structure from micro to millimeter scales, while scanning electron microscopy (SEM), atomic force microscopy (AFM) and transmission electron microscopy (TEM) give high resolution images down to the nanometer scale. Sample preparation, imaging principles, limitations, and representative results of each technique are discussed.

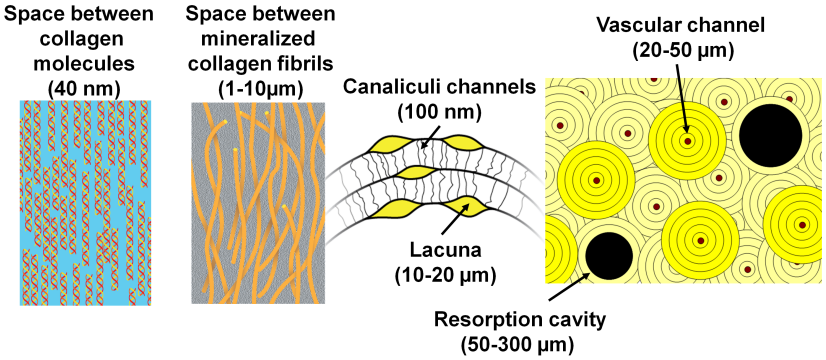

(a)

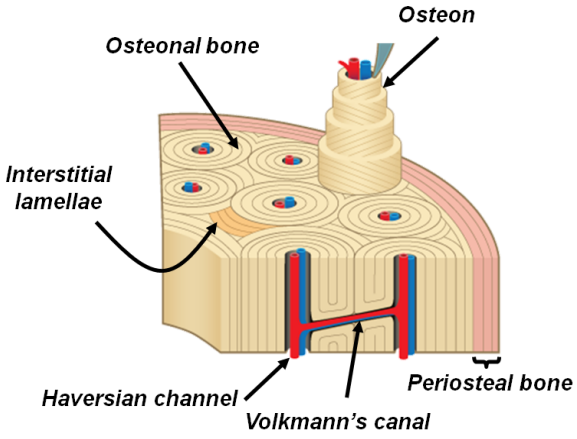

(b)

Figure 2.7: Porosity in bone: (a) The hierarchical structure of porosity. From left to right: spaces between wet collagen molecules, spaces between mineralized collagen fibers, canaliculi and lacuna spaces, vascular channels and resorption cavities. (b) Cross-section of cortical bone, showing vascular channels parallel and perpendicular (Volkmann's canals) to the growth direction.

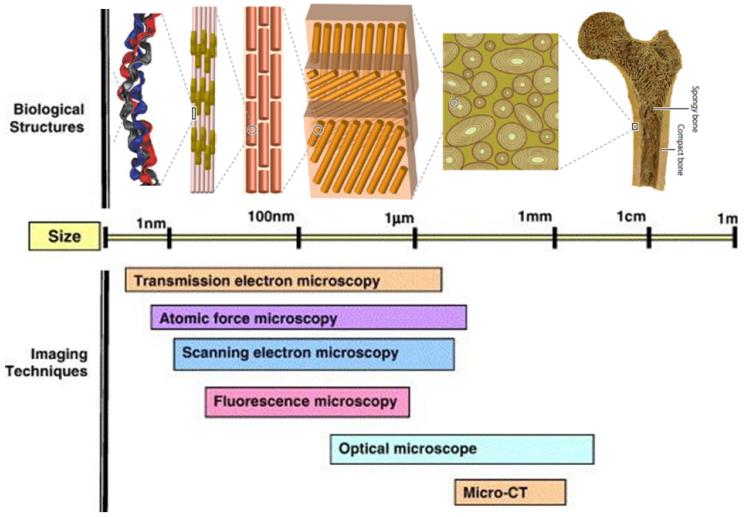

Figure 3.1: Imaging techniques that can be used to observe structural features of bone at varying hierarchical levels. Taken from Lim et al. (2006) and Launey et al. (2010). From left to right: helix tropocollagen molecule, mineralized collagen fibers, oriented stack of the collagen fibers, lamellar structure, osteonal structure, and whole bone.

3.1 Computed tomography (CT)

The X-ray computed tomography (CT) is an imaging method capable of reconstructing 3D internal structures of an object by X-ray projections from different viewing directions. It provides a map of the variation of X-ray absorption within the object, from which different phases of materials can be possibly identified and separated. The high-resolution X-ray CT (micro-CT) offers spatial resolution down to 1 μm where many microstructural features in engineering or biological materials could be investigated (Stock, 2003). Micro-CT provides additional advantages of noninvasive and nondestructive imaging, which minimizes sample preparation and can provide *in vivo* scans on live animals (Nolan et al., 2000; Waarsing et al., 2004; Oest et al., 2007). Compared with several other 3D microscopic techniques such as magnetic resonance imaging or ultrasound, micro-CT is most suitable to study bones and calcified tissues due to the high X-ray attenuation coefficient of calcium (Postnov et al., 2003). This technique is very useful in capturing trabecular bone architecture and gives rise to micro-CT based finite element models of trabecular bone, which we will discuss later in Section 6.

Micro-CT provides a stack of two-dimensional (2D) sliced gray images on which the 3D structure can be reconstructed. These gray values reflect combined influence of the bone mineralization level, the noise, and the partial volume effect, since a voxel in the resolution limit may contain both, bone and voids. One challenge is how to select a threshold to separate voids from bone components. After thresholding, the trabecular connectivity may be lost as some thin trabeculae are comparable to the 'density' of noise. Some improved techniques were developed to take account of local threshold segmentation (Waarsing et al., 2004; Buie et al., 2007). On the other hand, the gray-value may be directly transferred to 3D finite element models to provide an accurate prediction of elastic modulus (Homminga et al., 2001). Figure 3.2 shows a cartoon of different thresholding methods for trabecular bone, where the plain- and the mass-compensated thresholding (Ulrich et al., 1998) may lead to a loss of trabecular connectivity, while the direct gray-value models yield accurate predictions (Homminga et al., 2001). The gray-value can be also used

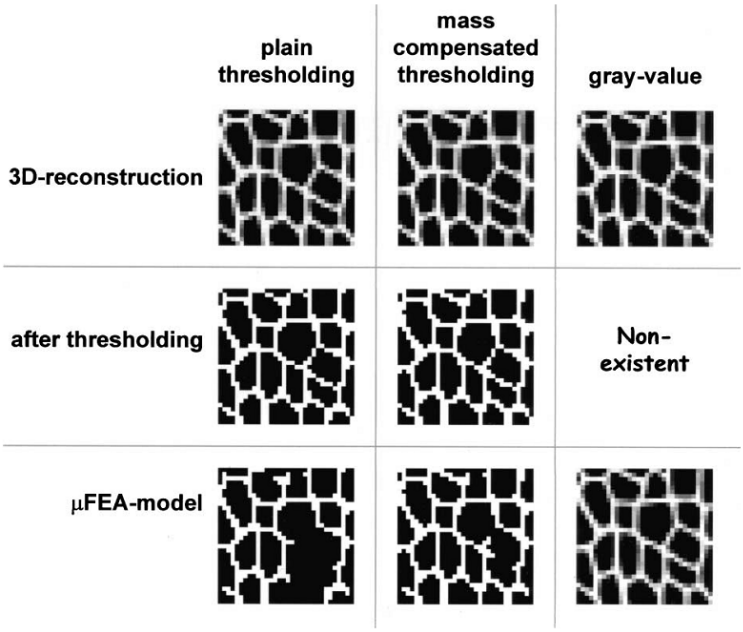

Figure 3.2: A cartoon of different methods regarding thresholding: plain thresholding, mass-compensated thresholding, and direct gray-value method (Homminga et al., 2001).

to calibrate the degree of mineralization in bone using certain mineral composite phantom (Deuerling et al., 2010). Some micro-CT artifacts exist in bone imaging,

especially the beam hardening effects (BHE), caused by the strong attenuation of soft X-rays to calcium. A metal filter is usually implemented to remove soft X-rays, while it degrades the signal-to-noise ratio (SNR). The synchrotron radiation based micro-CT can provide intense, laser-like X-rays to eliminate BHE and also obtain a high SNR (Ito, 2005), while it remains expensive and with restricted access. The contrast enhancement technique is important to delineate some microstructural details in micro-CT imaging. Recently a $BaSO_4$ stain was used to enhance contrast for the detection of microdamage in human cortical bone (Landrigan et al., 2011).

Table 3.1: Contribution of micro-CT to bone quantitative analysis (Odgaard, 1997; Schneider et al., 2007; Basillais et al., 2007).

Trabecular bone	Cortical bone
Relative bone volume (BV/TV)	Cortical bone volume density (Ct.BV/TV)
Bone surface to volume ratio (BS/BV)	Cortical thickness (Ct.Th)
Trabecular thickness (Tb.Th.)	Canal number density (N.Ca/Ct.TV)
Trabecular separation (Tb.Sp.)	Canal volume density (Ca.V/Ct.TV)
Trabecular number (Tb.N.)	Mean canal diameter ($\langle$ Ca.Dm $\rangle$), canal length ($\langle$ Ca. Le $\rangle$), canal orientation ($\langle$ Ca.$\theta\rangle$)
Trabecular pattern factor (TBPf)	Canal spacing (Ca.Sp)
Degree of anisotropy	Lacuna number density (N.Lc/Ct.TV)
Structure model index	Lacuna volume density (Lc.V/Ct.TV)
Fractal dimension	Degree of anisotropy
	Fractal dimension

TV = total volume

The ability to reconstruct 3D structure model by micro-CT allows a quantification of various 3D morphometric parameters for bone architecture, which provide

insights to the study of the structure-function relationship of bone. Table 3.1 summarizes the contribution of micro-CT to bone quantitative analysis. Note that in contrast to trabecular bone the characterization of cortical bone focuses on pores (canals and lacunae) rather than bone part.

The recent advancement of nano-CT provides higher resolution around several hundred to several tens nanometers and the osteocyte morphology in bone becomes open to study (Schneider et al., 2007; Hove, 2009). Figure 3.3 shows 2D sliced gray images and 3D reconstructed structure of a mouse cortical femur by nano-CT at 700 nm resolution (Schneider et al., 2007). The canal network and osteocyte lacunae are clearly identified and illustrated. 3D micro-CT data were validated by conventional 2D histology in a few studies (Müller et al., 1996; Ding et al., 1999; Basillais et al., 2007). The relation between morphometric parameters and mechanical properties has been successfully reported (Wachter et al., 2002; Schneider et al., 2007; Basillais et al., 2007).

3.2 Stereoscopy and optical microscopy (OM)

Stereoscopy is another prevailing imaging technique capable of generating 3D visualization and providing depth perception. The cellular structure of trabecular bone, particularly at the sub-millimeter scale, can be observed under stereoscope. Figure 3.4 is a stereoscopic image showing the longitudinal section of trabecular bovine femur (Chen et al., 2011). The trabecular network as well as the perforated plate structure with parallel aligned channels can be observed. Optical microscopy utilizes visible light that reflects from or transmits through the sample to allow a magnified view of the sample. For reflective light microscopy, bone samples are sectioned, mounted in epoxy, followed by grinding and polishing to produce smooth surfaces. Figure 3.5(a) shows a cross-sectional optical micrograph of cortical bovine femur taken in reflective light mode. Microstructural features, such as osteons (Os) (100-225 μm in diameter), interstitial bone, Haversian (H) and Volkmann's (V) canals (20-50 μm), and lacunae spaces (L) (10-20 μm) can be observed, as indicated in the micrograph. Transmitted light microscopy is widely applied in bone histology. Sample preparation requires fixation, dehydration, microtome-sectioning into slices 6-7 μm in thickness, and staining. Figure 3.5(b) is a transmitted optical micrograph of bovine femur stained with hematoxylin and eosin (H&E), a standard stain technique for histology. Optical micrographs show structural features at the micrometer scale; yet the resolution is limited to approximately 0.2 μm due to light diffraction, and therefore electron microscopy is required for imaging at higher magnifications.

3.3 Scanning electron microscopy (SEM)

SEM is a powerful technique imaging structural features of biological materials from micrometer down to nanometer length scales. The sample preparation for SEM is

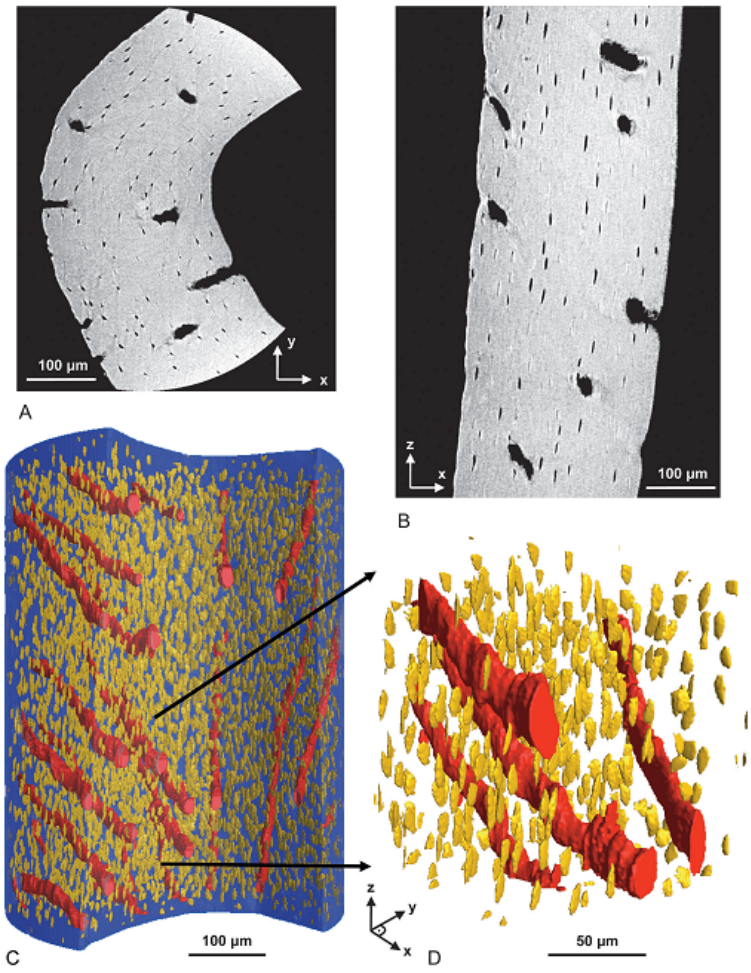

Figure 3.3: Nano-CT results of the lateral cortical mid-diaphysis of a mouse femur: the top row shows 2D sliced gray images in a transversal (A) and sagittal view (B). The bottom row represents the canal network (tubes in red) and osteocyte lacunae (prolate ellipsoids in yellow) within the same sample (Schneider et al., 2007).

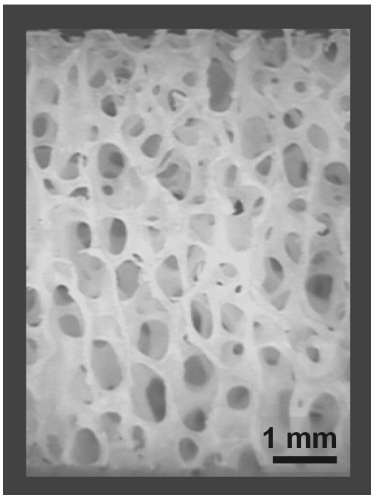

Figure 3.4: Stereoscopic image showing longitudinal view of trabecular bovine femur (Chen et al., 2011).

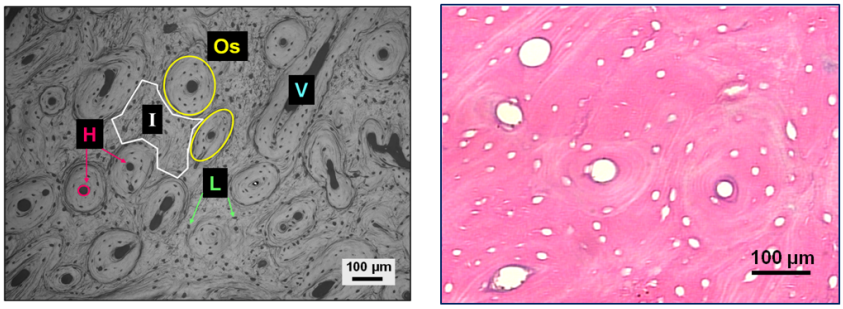

Figure 3.5: Cross-sectional optical micrograph in (a) reflective, and (b) transmitted light mode of cortical bovine femur showing microstructural features: osteons (Os), interstitial bone (I), lacuna spaces (L), Haversian (H) and Volkmann's (V) canals.

relatively easy compared with optical micrographs. Since biological materials are not conductive, it is necessary to coat a thin conductive layer on the samples before observation. There are two types of SEM images, secondary electron (SE) and backscattered electron (BSE) images. SE images provide information on surface morphology of the sample. Figure 3.6(a) is a secondary electron SEM micrograph showing the fracture surface of cortical bovine femur in the longitudinal direction. Lamellae with different collagen fiber orientation can be seen. Figure 3.6(b) shows a fracture surface with extensive collagen fiber pull-out. The mineralized collagen fibers are aligned in a preferred orientation along bone growth direction, and several bundles of fibrils 2-3 μm in diameter can be observed. BSE image shows contrast

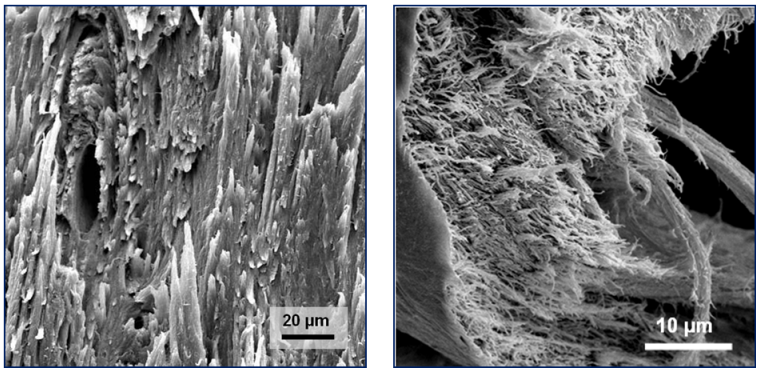

Figure 3.6: Secondary electron SEM micrographs of cortical bone showing: (a) lamellae with different collagen fibers orientation, and (b) mineralized collagen fibers.

in molecular weight of the sample. It is useful to distinguish difference in mineral (mostly calcium) content in bone. A BSE image of compact bovine femur is shown in Figure 3.7(a). The secondary osteons appear darker compared to the surrounding interstitial bone. The interstitial bone was found to have a higher mineral content which leads to higher elastic modulus and strength than secondary osteonal bone (Bonfield and Datta, 1974; Reilly et al., 1974b). Each secondary osteon is bounded by the cement line, an interface between secondary osteon and interstitial bone. Using quantitative BSE imaging, Skedros et al. (2006) showed that cement lines are more highly mineralized (collagen-deficient) compared with secondary osteons and interstitial bone, as shown in Figure 3.7(b). One of the concerns of imaging biological samples by SEM is the shrinkage and microcrack formation due to dehydration under high vacuum in SEM chamber. Critical point drying is a procedure unique to SEM sample preparation, which allows samples to be taken from the

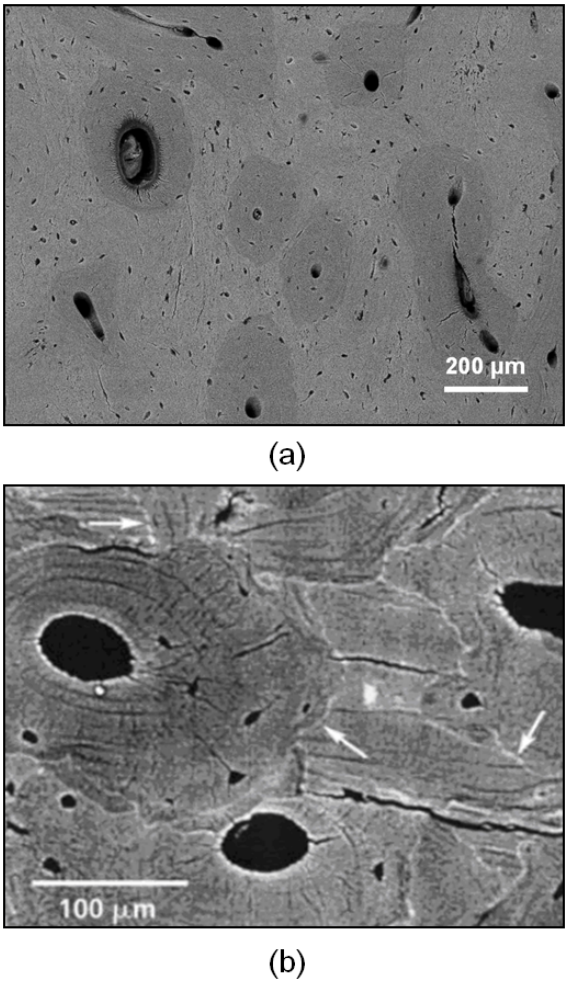

Figure 3.7: Backscattered electron (BSE) images showing cross-sectional microstructure of cortical bovine femur: (a) secondary osteons surrounded by interstitial bone; (b) the hyper-mineralized cement-line surrounding secondary osteons. Taken from Skedros et al. (2006).

liquid to the gas phase without any deleterious surface tension effect (Goldstein et al., 2003). An alternative approach is using environmental SEM, which allows the imaging of hydrated samples in a gaseous, relative low vacuum environment in the chamber. However, the resolution of micrographs taken in the environmental SEM is not as high as those taken in the high-vacuum condition.

3.4 Atomic force microscopy (AFM)

AFM is a high-resolution type of scanning probe microscopy with resolution on the order of fractions of a nanometer. The AFM consists of a cantilever with a sharp tip at its end, which is used to scan the specimen surface. AFM has been widely applied to characterize biological materials. Figure 3.8 shows an AFM image showing mineralized collagen fibrils in bone. The nanometer-sized granular mineral

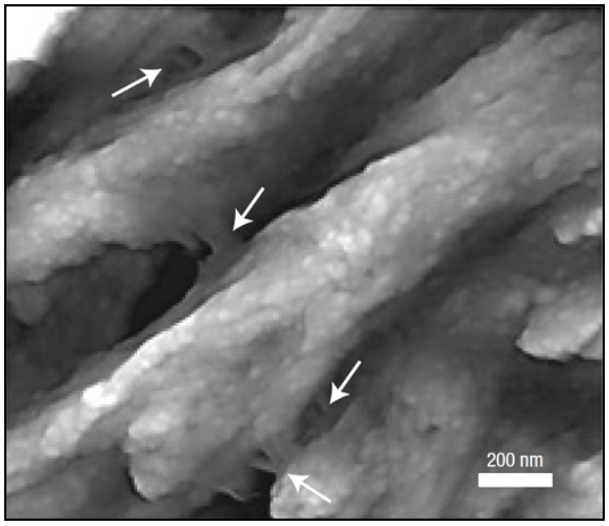

Figure 3.8: AFM image showing mineralized collagen fibrils in bone, arrows indicate the non-collagenous protein acting as glue between collagen fibrils. Taken from Fantner et al. (2005).

crystals on the surface of collagen fibrils and the NCPs (indicated by arrows) can be observed (Fantner et al., 2005). AFM has several advantages over SEM. AFM provides three-dimensional topography and higher resolution than SEM. Moreover, AFM can work perfectly in ambient air or aqueous environment without special sample preparation (e.g. metal coating) or ultra-high vacuum, which makes it possible to characterize biological materials and even living organisms. However, the single scan image size and depth of field of AFM are limited to 150 μm $\times$ 150

μm and 10-20 μm, respectively, much smaller than those of SEM, which are on the order of millimeters. Additionally, the scanning speed of AFM is slower than SEM, requiring several minutes for a single scan. Due to the nature of AFM tips, they cannot probe steep walls or overhangs, and therefore may cause artifacts.

3.5 Transmission electron microscopy (TEM)

TEM is capable of imaging at a significantly higher resolution (down to a single atom level) than optical and scanning electron methods. A TEM micrograph is formed from the interaction of the electrons transmitted through the specimen, magnified and focused onto an imaging device, such as fluorescent screen or CCD camera. TEM has been applied in structural characterization of bone at the molecular and nanometer length scales, such as the collagen fibrils and mineral crystallite previously shown in Figure 2.2 and Figure 2.3, respectively. TEM specimens are required to be thin enough, typically 60-100 nm, in order to let accelerated electrons travel through. Preparation of TEM specimens can be complex and time consuming, and is specific from specimen to specimen. In general, biological specimens need to go through serials of preparation steps, such as fixation, dehydration, polymerization, ultra-microtome sectioning, and staining before TEM observation.

TEM tomography provides three-dimensional structural information from tilt series with nanometer scale resolution. A relatively thick specimen ($\sim$ 250 nm) is required for TEM tomography, and therefore the high voltage ($\sim$ 400 kV) is required. Other than the standard preparation procedure, specimen is coated with 10 nm gold particles for further alignment. For single-tilt TEM tomography, a serial TEM images are taken from a range of tilting angles (-60 $^\circ$ to 60 $^\circ$) at certain step size. Figure 3.9(a) shows a series of representative TEM micrographs taken from the demineralized cortical antler bone at varying tilting angles (-60^o, -45^o, -30^o, -15^o, 0^o, +15^o, +30^o, +45^o, +60^o). The collagen fibrils $\sim$100 nm with periodic striations can be observed. Figure 3.9(b) is a maximum intensity projection (MIP) assembled from a series of TEM micrographs using the IMOD software. The three-dimensional structure of the collagen fibrils in cortical antler bone can be seen. The collagen fibrils are not parallel aligned; instead, some of them seem to be coiled together in a sinusoidal manner. Different orientations of fibril bundles can be observed. The majority of fibrils arrange diagonally ($\sim$30^o) on the surface and some fibrils beneath have slightly different orientation ($\sim$45^o). These results are very similar to the TEM observation of the human compact bone studied by Giraud-Guille (1988), who verified the twisted plywood architecture of collagen fibrils in bone.

Despite its ultra high resolution, there is a number of limitations and drawbacks of TEM technique. The sample preparation is relatively time consuming with a low throughput of samples. Moreover, the structure of the samples may be altered during the preparation process as well as damaged by the electron beam. Also, the field of view is relatively small compared with SEM, raising the concern that the characterized region may not be a representative of the whole sample.

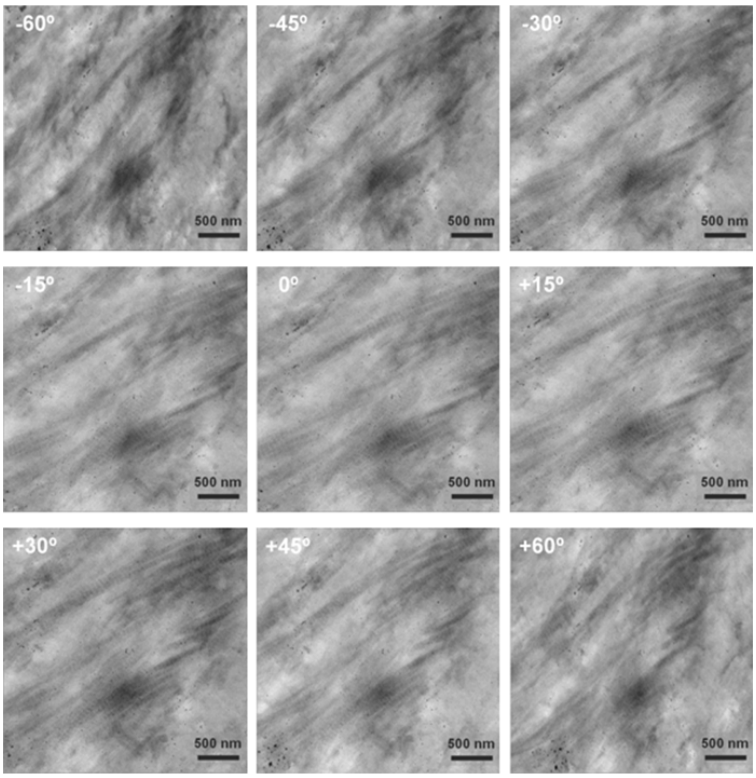

(a)

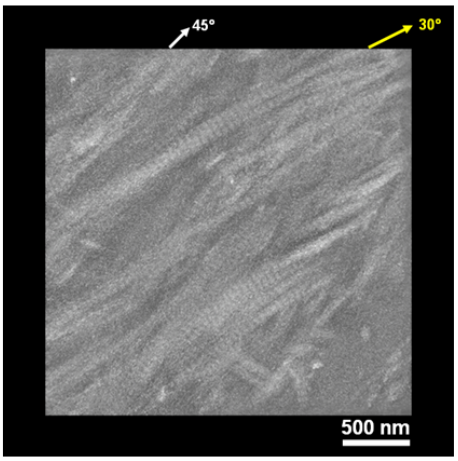

(b)

Figure 3.9: (a) A representative series of TEM micrographs of demineralized cortical antler taken at titling angles varying from -60 ° to +60 ° showing collagen fibrils. (b) The maximum intensity projection (MIP) showing the 3-dimensional structure of collagen fibrils in antler.

3.6 Confocal microscopy

Confocal laser microscopy has recently been applied to bone research, for example, *in vitro* fracture analysis. This technique is capable of imaging specifically labeled microstructural features, such as cracks and voids in bone and generating three-dimensional images by stacking micrographs obtained in incremental focal planes. O'Brien et al. (2000, 2002, 2003) used calcium binding fluorophores to label microcracks created during fatigue testing. Figure 3.10 shows confocal microscopy images taken of a notched equine femur tested in bending (Kulin et al., 2011). The test

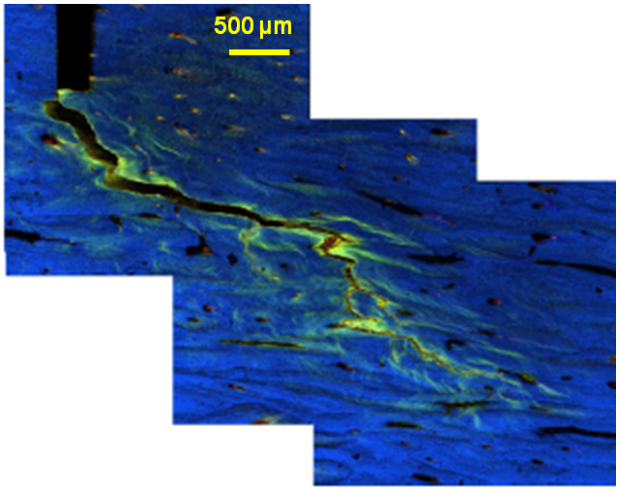

Figure 3.10: Confocal microscopy image of quasi-statically tested equine bone sample. Crack propagation is clearly seen in green. Taken from Kulin et al. (2011).

was stopped before complete failure. The fracture path and microcracks formation (labeled in green) can be clearly seen.

4 The elastic modulus of bone

Given the complexity of the bone structure, it is not surprising that values of elastic modulus (E) reported in the literature range from 5-34 GPa. The modulus is highly dependent on the species, mineral content (Currey, 1969b, 1990, 2010), age (Currey, 1996, 2004; Kulin et al., 2010), the amount of hydration (Nalla et al., 2005), amount of porosity (Mackenzie, 1950; Carter and Hayes, 1977; Bonfield and Clark, 1973), and anatomical location, e.g., rib vs. femur (Currey, 1990, 2010).

4.1 Effect of mineral content

The correlation between mechanical properties and the degree of mineralization from a wide variety of animal mineralized tissues has been investigated by Currey (1969b, 1990, 2010). Both the elastic modulus of bone and its toughness, measured by the area of the tensile stress-strain curve to failure, are strongly dependent on the degree of mineralization, as evident from Figure 4.1. In this plot, data from

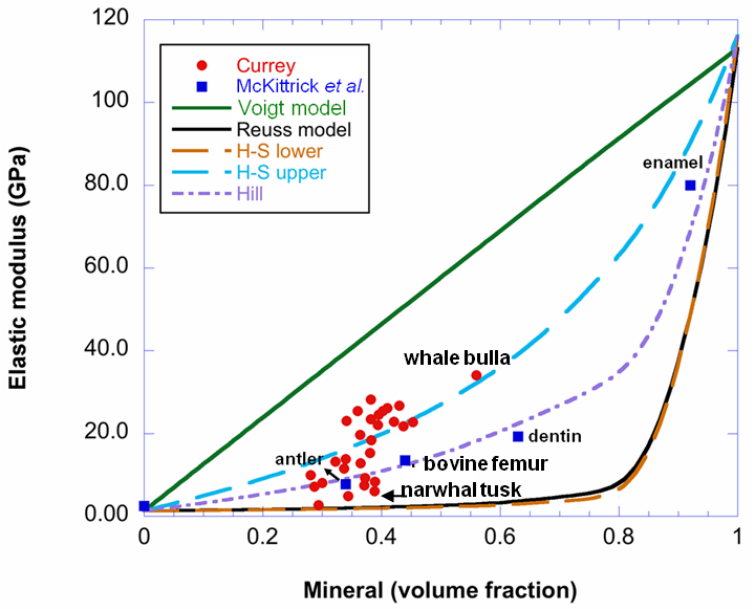

Figure 4.1: Effect of mineral volume fraction on elastic modulus of bones from various animals; data plotted from Currey (1990, 2010) and McKittrick et al. (2010). The Voigt, Reuss, Hashin-Shtrikman (H-S) upper and lower bounds, and Hill model curves are shown (see Section 6.1).

Currey (1990, 2010), taken from various mineralized tissues are plotted with data taken from McKittrick et al. (2010) for some other mineralized materials. Various composite model curves are shown (described in Section 6.1), demonstrating that these models do not adequately describe the elastic modulus. However, a general trend is observed with an increase in modulus with mineral content. The elastic modulus increases with mineral volume fraction in a roughly linear correlation. Antlers have a low degree of mineralization (left-hand side) with elastic modulus in the range of 7-10 GPa, while the elastic modulus for the highly mineralized whale bulla reaches 34 GPa. Interestingly, narwhal tusk cement is made of very loosely

organized bone, which leads to the lower modulus (about 5.5 GPa), although it is more highly mineralized than the antlers. Human enamel has the highest degree of mineralization, and corresponding elastic modulus is about 80 GPa.

4.2 Effect of porosity

The elastic modulus of cortical bone is known to be reduced by porosity. Carter and Hayes (1977) have proposed an expression for the elastic modulus that is proportional to the third power of the density,

$$E\alpha(1-p)^3, \tag{4.1}$$

where E is a measured elastic modulus and p is volume fraction of porosity.

Bonfield and Clark (1973) have expressed a modified Mackenzie (1950) equation to account for porosity as

$$E = E_o(1 - 1.9p + 0.9p^2), \tag{4.2}$$

where E_o is the elastic modulus of cortical bone tissue containing no porosity. This model can be applied to estimate the elastic modulus of cortical bone containing its porosity. For a compact bone containing 5% porosity, the absolute modulus E_o is 10% higher than the measured modulus, E; for a compact bone containing 10% porosity, E_o is $\sim$ 22% higher than E. However, this model fails to explain the anisotropy of bone.

For trabecular bone, elastic modulus is highly dependent on the amount of porosity (Gibson, 1985) and its architecture (rods versus struts, and their connectivity). Figure 4.2 shows the relative elastic modulus (E^*/E_s) as a function of the relative density(ρ^*/ρ_s). E_s and ρ_s are taken as 18 GPa and 1.8 gm/cm^3, respectively. The relative values are the measured ones (E^*, ρ^*) divided by values for a non-porous solid(E_s, ρ_s). The modulus fits the relationship

$$\frac{E^*}{E_s} = C\left(\frac{\rho^*}{\rho_s}\right)^2, \quad C = 1 \tag{4.3}$$

for trabecular bone taken from the femur, tibia and vertebrae. This relationship demonstrates that the elastic modulus of trabecular bone is strongly dependent on density.

4.3 Effect of orientation and anisotropy

The structure of bone is highly anisotropic: apatite crystals, collagen fibers and osteons are arranged in direction of the longitudinal axis of long bones. Therefore, bone exhibits anisotropic mechanical properties. The longitudinal elastic modulus and strength of cortical bone are higher than the transverse ones. The ratio of

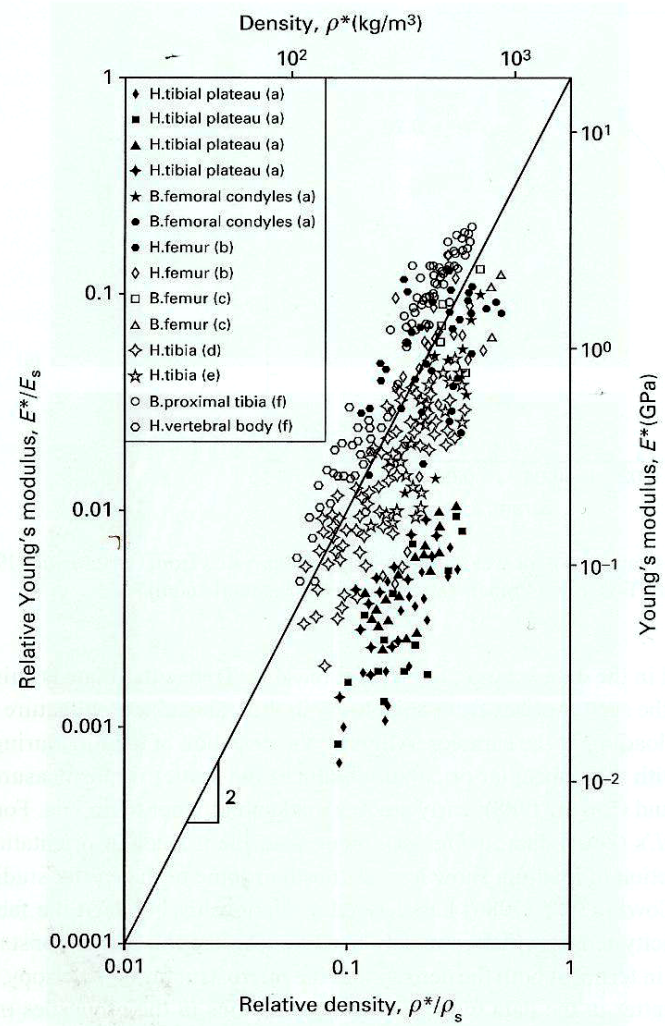

Figure 4.2: Relative elastic modulus as a function of relative density for trabecular bone. Taken from Gibson et al. (2010).

longitudinal/transverse elastic modulus varies from 1.6 to 2.4 (Bonfield and Clark, 1973; Bonfield and Grynpas, 1977; Currey, 2002). The elastic modulus of human compact bone in the longitudinal direction is reported to be in the range of 16-23 GPa; whereas in the transverse direction is about 6-13 GPa (Rho et al., 1998). Bonfield and Grynpas studied mechanical anisotropy of cortical bone at varying angles to the bone growth direction (longitudinal direction corresponded to 0°, transverse direction corresponded to 90°) by ultrasonic measurements. They found that elastic modulus gradually decreased with increasing angle (from 0° to 90°), and there was a plateau between 20° and 70°.

Figure 4.3 provides the tensile and compressive stress-strain curves for cortical bone in longitudinal and transverse directions (Lucas et al., 1999). The anisotropy

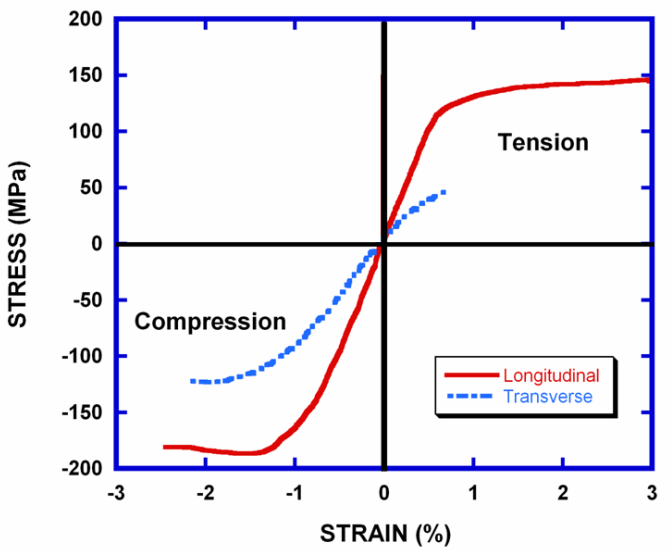

Figure 4.3: Tensile and compressive stress-strain curves for cortical bone in longitudinal and transverse directions. Adapted from Lucas et al. (1999).

is clearly visible – the elastic modulus in both tension and compression is higher for the longitudinal compared with the transverse direction. Other contributing factors to the anisotropy, besides the orientation of the collagen fibrils, are the mineral platelets and osteonal structure (in cortical bone), which also have a preferential orientation in the bone growth direction.

4.4 Effect of hydration

The amount of water present in bone is one of the most important determinants of its mechanical behavior. Bone is typically full of liquid, namely saline and blood, and the water in these mediums forms hydrogen bonds within the collagen structure. Bone has lower elastic modulus and strength yet higher strain to failure and toughness in hydrated state than in dry state. Bone can be re-hydrated with minimal effects on mechanical properties after drying. Similar results were also observed for dentin, another collagen-mineral composite found in teeth (Nalla et al., 2005). Poorly mineralized bones, such as antler and tortoise femur, have higher water contents, whereas highly mineralized bones (whale bulla) have lower water contents. This relates to the mineralization of the collagen fibrils, as minerals displace water within and around the gaps. The elastic modulus is usually up to 20% higher for dry compared with hydrated cortical bone and up to 40% higher for trabecular bone (Currey, 2002).

4.5 Effect of strain rate

The mechanical behavior of bone under dynamic loading has been of a great interest in the medical and engineering fields. Most bone fractures occur under dynamic loading from auto accidents, sporting injuries, or other catastrophic events. Due to the large amount of collagen content (40-45 vol. % for a femoral bone), bone is a highly viscoelastic material and the mechanical behavior is strain-rate sensitive. However, our understanding of the dynamic behavior of bone is far from complete. Most mechanical properties of bone found in literature were measured under quasi-static loading condition with a limited research performed dynamically.

One of the pioneers in the field of dynamic behavior of bone was McElhaney (1966) who tested hydrated human compact bone in compression at strain rates varying from 10^{-3} to 1500 sec^{-1}. An air-gun type machine was used, capable of performing strain rates up to 4000 sec^{-1}. The compressive stress-strain curves showed that both elastic modulus and ultimate compressive stress increased with increasing strain rates while the strain to failure decreased (Figure 4.4). Tennyson et al. (1972) tested the dynamic response of bovine femur using the split-pressure Hopkinson bar (SPHB) at strain rates in the range of 10 - 450 sec^{-1}, in both hydrated and dehydrated conditions and found similar trends for both hydration states. Lewis and Goldsmith (1975) measured the dynamic mechanical properties of bovine bone in compression, tension, and torsion by using a biaxial split Hopkinson pressure bar combined with strain gages. The results showed further evidence of the viscoelastic behavior of bone. Kulin et al. (2010) investigated the dynamic response of compact equine bone and corroborated the results of McElhaney (1966), showing the increasing elastic modulus and compressive strength with the strain rate.

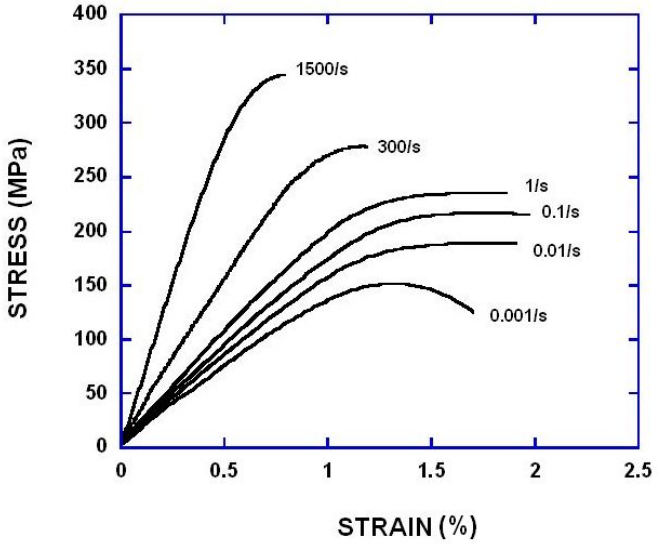

Figure 4.4: Compressive stress-strain curves for human cortical bone at varying strain rates. Reproduced from McElhaney (1966).

4.6 Age effect

The bone mineral density (BMD) changes significantly with age and the elastic modulus should change accordingly. Currey (2004) showed that bone becomes more mineralized with increasing age, therefore getting more stiff and strong. For example, the elastic modulus of a human femur of 35-year old bone was twice that of 3-year old. Figure 4.5(a) shows the BMD from the lumbar spine as a function of age for young girls (Boot et. al, 1997), demonstrating that mineralization occurs steadily from 7 to 18 years, at which point the BMD levels out. In Figure 4.5(b), BMD is plotted for women from ages 20-80 (Riggs et. al, 1981), clearly showing the mineral fraction in bone is monotonically decreasing. This significant decrease is especially troublesome in middle age and older populations, where osteoporotic fracture can occur. Osteoporosis is a common disease that causes a lower bone mass density. This is particularly acute in trabecular bone, where these losses result in disruptions of the trabecular network creating uncharacteristically large voids that are much more susceptible to fracture (e.g., Bouxsein, 2008; Lubarda et al., 2011).

It has been shown that several other factors, like degradation of collagen with age (Danielsen et al., 1994), or larger density of un-remodeled microcracks (Currey et al., 1996), could have an effect on the age-related mechanical properties. Several interesting results about the age related changes of bone microstructure and its

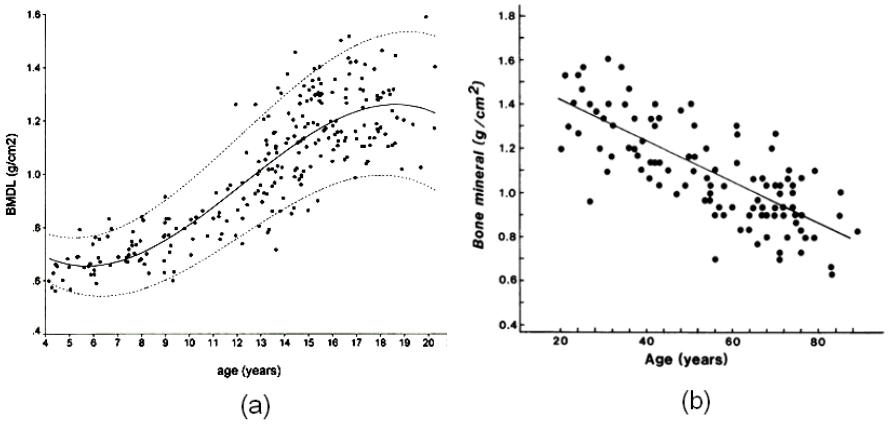

Figure 4.5: Bone mineral density (BMD) from the lumbar spine as a function of age for: (a) young girls (Boot et al., 1997), and (b) older women (Riggs et al., 1981).

influence on bone toughening mechanisms were reported by Nalla et al. (2006), and Ritchie et al. (2006). They attributed the fracture receptivity of aged bones to an increasing density of Haversian systems and changes in collagen cross-linking at the nanoscale level.

5 Experimental methods to measure elastic modulus

There are many methods to investigate the mechanical properties of bone. Extrinsic parameters (e.g. fracture stress and strain) depend on the actual sample size and testing method, thus being different for the different sized samples. Intrinsic parameters, such as compressive stress and strain, are calculated based on the actual sample dimensions and are usually similar for the different sized samples.

Tests can be classified as non-destructive and destructive tests. The two main non-destructive methods are based on ultrasound and nanoindentation techniques. Compression, bending, torsion, and tension are the most widely used destructive tests.

5.1 Basic measurements

One of the most important factors that should be considered before doing any mechanical testing is the specimen storage and preparation technique. Hydration plays an important role for all biological materials. Bone can be stored for periods of up to eight months at $\leq -20^o$ C, although repeated freezing and thawing should be avoided (An, 1999). Bone can be dried and rehydrated without significantly affecting its elastic properties; however, the toughness could be altered (Currey, 1988b). For all mechanical tests, bone needs to be tested in the hydrated condition. This involves soaking the specimens in an aqueous solution, such as Hank's buffered saline solution, for a period of several hours or overnight, depending on the size of the sample. Measurements on dry samples do not adequately reflect the nature of bone, since in the body bone is filled with fluid.

Before testing a bone, several basic experiments need to be performed: drying for water content and ashing for mineral content. Weighing the hydrated sample under ambient condition, then drying in an oven ($\sim 105^o$C) to remove the water and subsequent re-weighing will give the weight fraction of water. Ashing involves baking the bone at higher temperature ($\sim 550^o$C) to remove all of the organic material. The weight before and after ashing gives the weight fraction of the mineral phase. These are two key measurements that must be reported for experimental procedures.

Another basic measurement is density. Because the elastic modulus is extremely sensitive to the amount of porosity, density needs to be quantified. The density of collagen is 1.35 gm/cm^3 and the density of hydroxyapatite is 3.15 gm/cm^3, and with these numbers, the volume fraction of proteins, mineral and water can be determined. Although the NCPs have a slightly different molecular weight than collagen, the volume fraction is low and estimates based on collagen only are adequate.

5.2 Non-destructive methods

5.2.1 Ultrasound

Ultrasound measurements involve the evaluation of the elastic modulus, which is proportional to the sample density (ρ) and the velocity of sound (υ):

$$E = \rho \upsilon^2. \tag{5.1}$$

According to Cowin (2001) this equation can be used if ultrasonic wavelength is greater than the cross-sectional dimension of the sample and characteristic dimension of the structure (for example, the size of the osteon), in order for the wave to propagate through the specimen. Another difficulty is related to the anisotropic and non-uniform bone properties. The density of bone samples varies depending

on the anatomical position; therefore, estimation of the elastic modulus by ultrasound technique usually provides very scattered results for different bone locations. However, a great advantage of ultrasound technique is that it does not require expensive equipment (Turner and Burr, 1993), and it does not destroy the specimen. The equipment usually involves ultrasonic pulse generator, oscilloscope, and wave transducers. An additional significant benefit of the ultrasound technique is that the anisotropic elastic properties can be measured using the same sample by propagating the waves along the different directions.

5.2.2 Nanoindentation

Nanoindentation is a technique in which a known load (in the 0.25 mN – 5 N range) from a pointed diamond indenter (tip radius $\sim$ 100 nm) is applied onto the surface of the material. The hardness is related to the load (P) and indentation depth (h), but sensitive positioning sensors allow for measurement of the loading and unloading curve. The 'stiffness' (S) is given as the slope of the unloading curve (dP/dh), as shown in Figure 5.1(a). The reduced modulus, E_r, is calculated from:

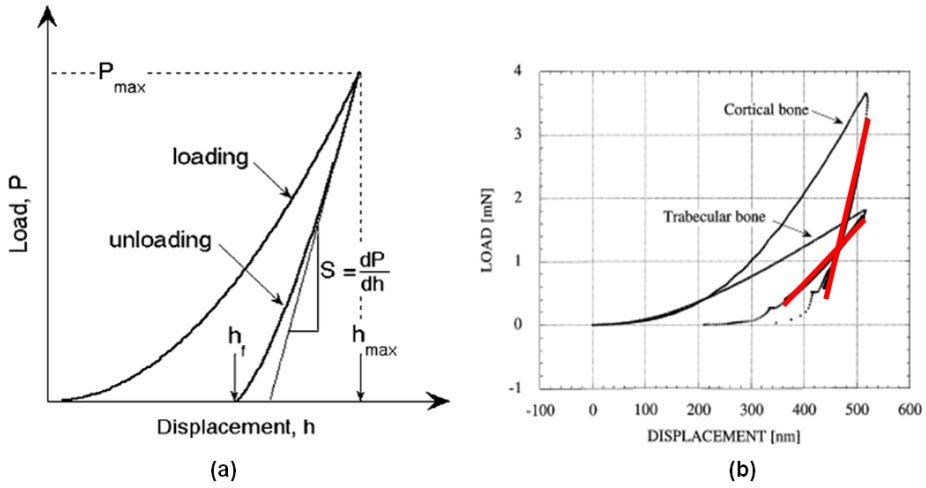

Figure 5.1: (a) Illustration of important measured nanoindentation parameters: maximum load (P_{max}), maximum displacement (h_{max}), and the elastic unloading stiffness (S). Taken from Oliver and Pharr (2004). (b) Typical nanoindentation curves for cortical and trabecular bone samples. Elastic modulus is estimated from the slope (red lines) of the liner parts of unloading portions of the curves. Taken from Zysset et al. (1999).

$$E_r = \frac{1}{\beta}\frac{\sqrt{\pi}}{2}\frac{S}{\sqrt{A_p(h_c)}}, \tag{5.2}$$

where β is a geometrical parameter that depends on tip geometry, and $A_p(h_c)$ is the projected area of indentation at contact depth h_c. The elastic modulus of the sample, E_s, is related to E_r and the elastic constants of the diamond indenter (E_i and ν_i) by:

$$\frac{1}{E_r} = \frac{\left(1-\nu_s^2\right)}{E_s} + \frac{\left(1-\nu_i^2\right)}{E_i}. \tag{5.3}$$

The indices s and i correspond to the sample and the indenter, respectively. The modulus E_s can be evaluated from Eq. (5.3) after the reduced modulus calculated from Eq. (5.2). Despite the name, the indented boundaries are in the range of 1-10 μm. The osteonal and interstitial lamellar regions of bone can be probed separately.

Figure 5.1(b) shows the nanoindentation curves for cortical and trabecular bone. The elastic modulus is shown to be lower for trabecular than cortical bone samples, due to the high degree of porosity of the trabecular samples. In the figure, the red lines show the portion of the loading/unloading curve that is used for estimating S.

The elastic properties of microstructural components in human femur bone using nanoindentation have been investigated by several groups. Rho et al. (1999) showed that elastic modulus of interstitial lamellae ($\sim$ 26 GPa) was higher than that of the osteons ($\sim$ 22 GPa) in the longitudinal direction for human femur cortical bone. Zysset et al. (1999) investigated properties of cortical and trabecular human femoral bone at several locations. They pointed out that elastic modulus was higher for interstitial lamellae than for osteonal part for both diaphyseal and neck regions of femoral bone. The interstitial lamellae show a higher elastic modulus than the osteonal region due to the higher mineral content. This is clearly shown in the BSE SEM image in Figure 3.7(a), where the interstitial lamellae are brighter, indicating a higher calcium (mineral) content.

A comprehensive review of bone properties measured by nanoindentation technique was outlined by Thurner (2009). He summarized the results from the nanoindentation experiments of different human and animal bones, including tibia, femur, and vertebra. It was shown that although nanoindentation is a powerful method for the evaluation of elastic properties, hardness, viscosity and plastic deformation of bone, this procedure is very sensitive to a sample preparation technique and testing conditions. For example, according to Thurner (2009), elastic modulus of human femur middle portion varied between 17 and 27 GPa, depending on sample hydration conditions, maximum applied force, tip type, and anatomical direction. Thus, it is crucial to report the exact experimental methods used to prepare bone for nanoindentation experiments.

The AFM can also be used as a nanoindenter (Balooch et al., 2005; Tai et al., 2007). The tip is made from silicon and is much finer and smaller than the diamond

tips used for standard nanoindentation methods (tip size $\sim$ 15 nm). However the maximum load that can be applied is much smaller. This method has been used to determine the elastic modulus of cortical bone from various regions in one sample in which values from 2-30 GPa were measured (Tai et al., 2007). This wide range was attributed to nanoscale irregularities, which were also proposed as the origin of bone toughness.

5.2.3 Microindentation

An interesting application of *in vivo* indentation has been developed by Hansma et al. (2006, 2008). Bone material properties can be measured directly on a patient through the skin or other soft tissue. The typical bone diagnostic instrument (BDI) invented by Hansma group is shown in Figure 5.2. It consists of a reference

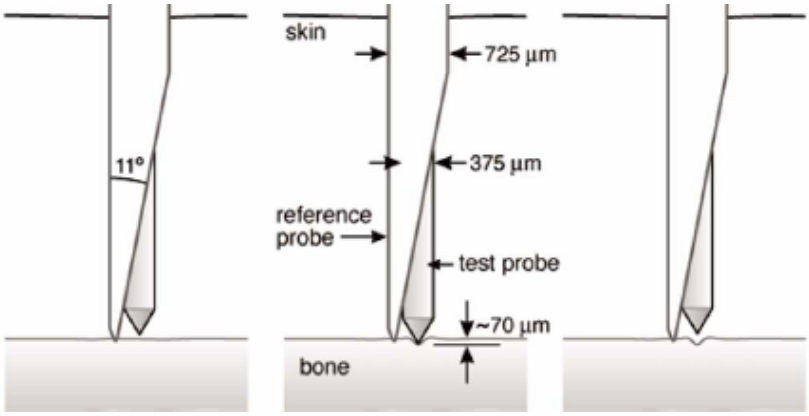

Figure 5.2: The probe assembly for bone diagnostic instrument. It consists of the reference probe and the test probe. Taken from Hansma et al. (2008).

probe and a test probe (with radius of 2.5 μm). A test probe is inserted into a bone through the skin and other connective tissues; an indented distance is usually about several microns, measured relatively to a reference probe. The whole test takes several minutes and requires only minor local anesthetization. The BDI provides the information about bone material properties *in vivo*, and moreover is able to measure the continuing damage that results from a repeated loading. BDI works in two different modes: force controlled and distance controlled. Penetration distance (corresponding to a fixed loading force), or force (corresponding to a fixed penetration distance) were measured for the patients with different expected fracture properties (based on the age). It was found that older bones were less capable of accumulating damage in form of microcracks and are associated with increasing risk of fracture.

5.2.4 Electronic speckle pattern interferometry (ESPI)

Zhang et al. (2001) and Barak et al. (2009) described an interesting method to evaluate the elastic properties of bone: electronic speckle pattern interferometry (ESPI). ESPI is an optical method that produces strain maps of the whole sample loaded in bending, as shown in Figure 5.3. According to these authors this method

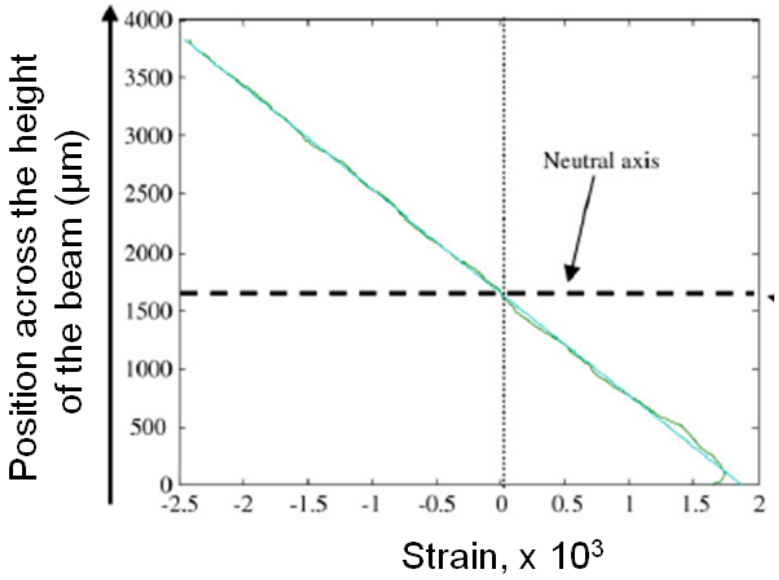

Figure 5.3: Strain distribution across the height of the beam determined by electronic speckle pattern interferometry (ESPI) for four-point bending. Taken from Barak et al. (2009).

is less sensitive to sample surface quality and provides excellent information about the bone elastic modulus. Barak et al. (2009) used ESPI to precisely determine the tensile and compressive strains through the thickness of the cortical bone specimens tested in four-point bending. This information was used for the evaluation of the tensile and compressive elastic constants. It was found that tensile elastic modulus of mature equine osteonal bone is 6% higher than compressive elastic modulus. They mainly attributed their result to the structural inhomogeneities (see Section 5.3.2).

5.3 Destructive methods

Turner and Burr (1993) and Beaupied et al. (2007) summarized the main destructive mechanical tests. They pointed out that in each case the mechanical test should be selected based on the bone nature (cortical or trabecular), its geometric parameters, and the loads that bone experiences *in vivo,* in order to minimize the errors in the determination of the mechanical properties.

5.3.1 Flexure

Flexure tests are widely used due to the ease of sample preparation. For three-point bending tests, the stress distribution is non-uniform across the thickness and along the length of the bone sample (Figure 5.4(a)). The elastic modulus $\left(E_{(3)}\right)$ can be

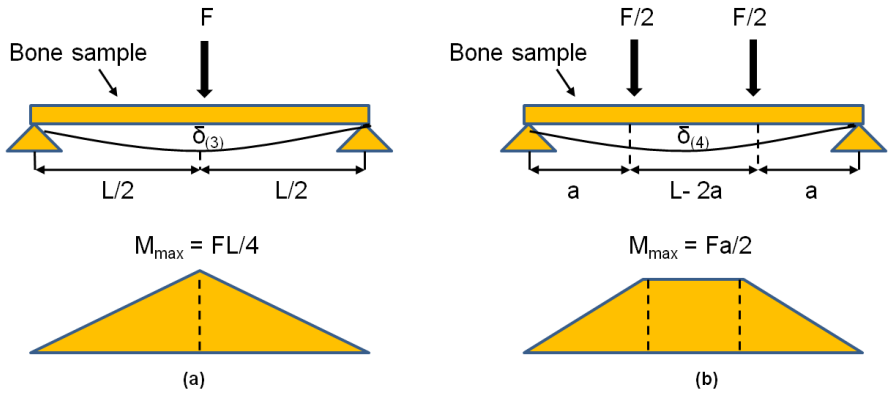

Figure 5.4: The bending moment distribution for: (a) three-point bending, and (b) four-point bending tests.

extracted from this test as

$$E_{(3)} = \frac{FL^3}{4\delta_{(3)}bh^3}, \tag{5.4}$$

where F is the applied load, L is the span between bending fixtures, b is the sample width, h is the sample height, and $\delta_{(3)}$ is the maximum deflection at the midpoint of the sample.

To avoid the non-uniform bending moment, several groups (Keller et al, 1990; Draper and Goodship, 2003) employed a four-point bending test that is characterized by a constant bending moment between the applied loads (Figure 5.4(b)). The

elastic modulus $\left(E_{(4)}\right)$ is given by

$$E_{(4)} = \frac{FL^3}{4\delta_{(4)}bh^3}\frac{a}{L}\left[3 - \left(\frac{2a}{L}\right)^2\right], \tag{5.5}$$

where a is the distance between the fixture and the applied load. The elastic modulus obtained from the four-point bending test $E_{(4)}$ can be related to the elastic modulus obtained from the three-point bending test $E_{(3)}$ by

$$\begin{aligned} E_{(4)} &= \kappa_\upsilon E_{(3)}\frac{\delta_{(3)}}{\delta_{(4)}} \\ \kappa_\upsilon &= \frac{a}{L}\left[3 - \left(\frac{2a}{L}\right)^2\right] \end{aligned} \tag{5.6}$$

Clearly, if $a = L/2$, the geometric factor $\kappa_\upsilon = 1$, because in this configuration the four-point bending test reduces to the three-point bending test, so that $\delta_{(4)} = \delta_{(3)}$.

5.3.2 Tension and compression tests

Bone is typically loaded in compression, thus much attention has been devoted to compressive properties. However, bone is most likely to fracture by shear, in which failure is initiated by the tensile stresses. Thus, the elastic and plastic response of bone under a wide variety of loading conditions is of interest. Novitskaya et. al. (2011) investigated the mechanical properties of cortical bovine bone in compression in three anatomical directions that showed highly anisotropic properties. Figure 5.5 shows the stress-strain curves for bovine cortical bone tested in compression for three anatomical directions, demonstrating that the longitudinal direction is the stiffest bone direction due to preferential orientation of collagen fibers and mineral crystals in this direction.

Mechanical properties obtained from the tension and compression experiments are expected to be similar. Recently, however, Barack et al. (2009) investigated the secondary osteonal equine bone properties obtained by ESPI and four-point bending tests, and found that the tensile elastic modulus was $\sim 6\%$ higher than compressive one. They attributed their result to the structural inhomogeneities (due to possible differences in mineralization and porosity concentration) of bone samples. On the other hand, these results should be viewed by taking into account the size effect, because the structural hierarchy exists at all length scales, so that smaller samples are more sensitive to the presence of inhomogenieties.

The elastic modulus strongly depends on the bone anatomy (Currey 2004, 2010). A comprehensive review of mechanical properties of femur bone from seven main vertebrate groups (including birds, reptiles, and mammals) from the evolutionary point of view was given by Erickson et al. (2002). They tested the whole

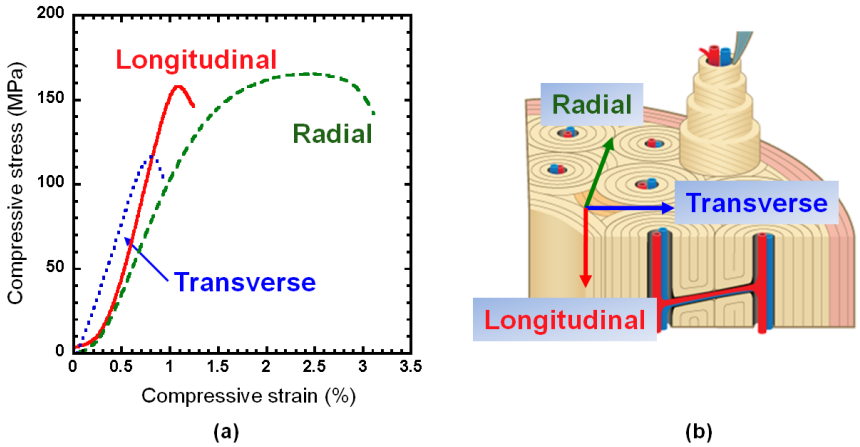

Figure 5.5: (a) Compressive stress-strain curves for bovine cortical bone for three anatomical directions. (b) The longitudinal direction is clearly the stiffest bone direction, while the radial one has the maximum toughness. Modified from Novitskaya et al. (2011).

femur bone of 69 species from different animal groups by three-point bending tests and analyzed their results in an evolutionary context using phylogenetic character analysis. The average elastic modulus was found to be 22.2 $\pm$ 6.7 GPa for all animals tested. It was concluded that material properties of femur bone were not changed much during evolution. On the other hand, Currey (1990, 2004, 2010) found a wide variety of elastic moduli for different animal specimens that increased with the mineral fraction. Animal specimens for these studies, including such rare ones as whale bulla, tortoise bones, fish scale, and penguin bones, came from the different sources and anatomical locations (femur, tibia, radius, rib, bulla), so that the results show even wider range of values of the elastic modulus (between 2.7 GPa for dolphin ulna and 34.1 GPa for whale bulla).

Table 5.1 and Table 5.2 summarize the results of recent reported measurements of the elastic modulus obtained by different experimental techniques for cortical and trabecular bovine and human femur bone.

Table 5.1: Elastic modulus of cortical femoral bone.

Test method	Elastic modulus, GPa	Reference	Type	Condition
Compression	(16.2 - 17.0)[a]	Keller (1994)	Human	Wet
	19.9 ± 1.8	Bayraktar et al. (2004)	Human	Wet
	22.6 ± 1.2	Novitskaya et al. (2011)	Bovine	Wet
Tension	16.6 ± 1.8	Dong and Guo (2004)	Human	Wet
	16.7[b]	Currey (2004)	Human	Wet
	24.5[b]	Currey (2004)	Bovine	Wet
Torsion	4.7 ± 0.7 (shear modulus)	Dong and Guo (2004)	Human	Wet
4-point bending	12.3 ± 1.7	Keller et al. (1990)	Human[c]	Wet
	19.8[b]	Draper and Goodship (2003)		Wet
3-point bending	17.3± 1.3	Grimal et al.(2009)	Human	Wet
	13.5[b]	Currey (1999)	Bovine	Wet
	18.6 ± 1.9	Cuppone et al. (2004)	Human	Wet
	24.2[b]	Zioupos et al. (2000)	Bovine	Wet
Ultrasound	13.9[b]	Rho et al. (1995)	Human	Wet
	32.5 ± 0.5	Hunt et al. (1998)	Human	Fresh
	22.1 ± 1.1	Grimal et al. (2009)	Human	Wet
	20.5 ± 0.2	Turner et al. (1999)	Human	Wet
	41.0 ± 3.0	Zimmerman et al. (1994)	Bovine	Dry
Interferometry	19.8 ± 1.1	Zhang et al. (2001)	Bovine	Wet
Nanoindentation	20.1 ± 5.4	Zysset et al. (1999)	Human	Wet
	23.5 ± 0.2	Turner et al. (1999)	Human	Wet

[a] – only range reported
[b] – only number reported
[c] – the type was not reported

The results obtained by non-destructive methods are higher than those from destructive methods. However, it should be pointed out that nanoindentation measures the local properties of bone samples close to the sample surface (Turner et al., 1999; Zysset et al., 1999), so that these results should not be directly compared to those that measure bulk properties. Additionally, nanoindentation is not as influenced by porosity, as are the bulk measurements.

Table 5.2: Elastic modulus of trabecular femoral bone.

Test method	Elastic modulus, GPa	Reference	Type	Condition
Compression	1.4 ± 0.3	Lubarda et al. (2011)	Bovine	Dry
	0.44 ± 0.27	Lotz et al. (1990)	Human	Wet
Tension	2.4 ± 0.8	Morgan et al. (2001)	Human	Wet
Torsion	0.29 ± 0.18 (shear modulus)	Bruyere Garnier et al. (1999)	Human	Wet
Ultrasound	1.3[b]	Rho et al. (1995)	Human	Wet
	17.5 ± 1.1	Turner et al. (1999)	Human	Wet
Ultrasound + FEA*	4.5 ± 0.7	van Lenthe et al. (2001)	Bovine	Wet
Nanoindentation	11.4 ± 5.6	Zysset et al. (1999)	Human	Wet
	18.1 ± 1.7	Turner et al. (1999)	Human	Fixed

[b] – only number reported
FEA* - microfinite element analysis

On the other hand, the good agreement between the results for different destructive methods for both cortical and trabecular bones is clearly seen from Tables 5.1 and 5.2. The average elastic modulus for all destructive methods was 17.5 ± 2.9 GPa for femur cortical bone, and 1.4 ± 0.8 GPa for femur trabecular bone. For non-destructive methods these numbers were 21.8 ± 5.2 GPa for femur cortical bone and 15.7 ± 3.0 GPa for femur trabecular one. The values of elastic modulus for destructive and non-destructive methods vary significantly for trabecular bone, but differ only by 20% for cortical bone. This could be explained by the more uniform density and porosity distributions in cortical as compared with trabecular bone.

Mechanical properties of bone are usually measured under the wet condition (formalin, water, saline solutions), because bone is always wet *in vivo*. As men-

tioned earlier, bone has lower elastic modulus and strength but higher strain to failure and toughness in hydrated state than in dry state (Zimmerman et al., 1994; Nalla et al., 2005). This is due to the wetting of collagen fibers that make a contribution to the whole bone behavior. Water plasticizes the collagen matrix, filling interior pores, and therefore decreases the elastic modulus of the whole bone (see Section 2.1.3).

Differences in the elastic modulus measured by the same techniques, and even under the same hydration conditions, can be explained by the different microstructure between osteonal and other types of cortical bone, the age of the tissue, and the position of the sample along the femur bone (i.e. neck, head, or diaphysis).

6 Modeling methods to predict elastic properties of bone at different hierarchical scales

Various analytical and computational techniques were used to study the elastic behavior of bone as a composite material with hierarchical structure. One could classify them into the following four different categories of models available in the literature:

- Models based on strength of materials;
- Models based on micromechanics theories;
- Computational models mostly using FEM;
- Atomistic simulations using molecular dynamics (MD).

Each of the above-mentioned models has some advantages and disadvantages. Strength of materials models are approximate but simpler in formulation, and have been used to account only for two main constituents of bone, namely collagen and hydroxyapatite (HA). Micromechanical models usually involve more rigorous elastic solutions and have been used to capture all bone's constituents through a step-by-step homogenization scheme. However, they still include simplifying geometry and assumptions. For example, the effect of collagen cross-links, collagen-HA interphase, and geometrical arrangement of collagen and HA with respect to each other are difficult to be addressed in micromechanics-based models. These shortcomings can be addressed by using FEM models. MD simulations can shed light on behavior of bone at nanoscale and provide some required inputs for FEM such as properties of collagen cross-links and collagen-HA interphase. In this section we will discuss the assumptions, limitations, and drawbacks of all these approaches. Such discussion may help to develop inclusive models which can address various physical, mechanical, and biological aspects of bone behavior at different scales.

Throughout the following sections E, ν, G, $\mathbf{C}$, and Φ denote, respectively, elastic modulus, Poisson's ratio, shear modulus, elastic stiffness tensor, and volume

fraction of a pertinent phase. Also, subscripts "col", "HA", "m", and "f" refer to collagen, HA, matrix, and fibers, respectively. Furthermore, E_l shows the effective longitudinal elastic modulus of bone at a corresponding scale, while E_t is its effective transverse modulus. **S** is the fourth-order Eshelby tensor which depends on matrix elastic constants and inclusion geometry (Eshelby, 1957).

6.1 Modeling of bone as a two-phase composite

Models based on strength of materials are mainly variants of Voigt (1889) and Reuss (1929) bounds . Most of such methods were originally proposed for modeling of two-phase composites rather than bone. However, they can also be applied to model a mineralized collagen fibril as a collagen-hydroxyapatite composite. Note that originally such models did not distinguish between different hierarchical scales in bone and were proposed to model bone in general. Voigt assumed the material to be composed of alternating layers of matrix and fiber under uniform strain. Using this model, the longitudinal elastic modulus of bone is predicted to be

$$E_l = \Phi_{\text{col}} E_{\text{col}} + \Phi_{HA} E_{HA}. \tag{6.1}$$

On the other hand, Reuss assumed the condition of parallel layers under uniform stress, and evaluated the effective transverse elastic modulus of composite (bone, in this case) as

$$\frac{1}{E_t} = \frac{\Phi_{col}}{E_{\text{col}}} + \frac{\Phi_{HA}}{E_{HA}}. \tag{6.2}$$

Voigt and Reuss models provide the upper and lower bounds for the elastic modulus of a composite material simply based on the relative volume fractions of the constituents. However, more refined bounds of the elastic properties of a composite can be found using a model proposed by Hashin and Shtrikman (1963). This model is based on a variational principle originally formulated for the elastic properties of a 3D isotropic composite with arbitrary phase geometry. Using this model, the lower and upper bounds on bone bulk modulus, k_{H-S}^{lower} and k_{H-S}^{upper}, and shear modulus, G_{H-S}^{lower} and G_{H-S}^{upper}, are defined as

$$\begin{aligned} k_{H-S}^{lower} &= k_{col} + \frac{\Phi_{HA}}{\dfrac{1}{k_{HA}-k_{col}} + \dfrac{3\Phi_{col}}{3k_{col}+4G_{col}}}, \\ k_{H-S}^{upper} &= k_{HA} + \frac{\Phi_{col}}{\dfrac{1}{k_{col}-k_{HA}} + \dfrac{3\Phi_{HA}}{3k_{HA}+4G_{HA}}}, \end{aligned}$$

$$G_{H-S}^{lower} = G_{col} + \frac{\Phi_{HA}}{\dfrac{1}{G_{HA}-G_{col}} + \dfrac{6\Phi_{col}(k_{col}+2G_{col})}{5G_{col}(3k_{col}+4G_{col})}}, \tag{6.3}$$

$$G_{H-S}^{upper} = G_{HA} + \frac{\Phi_{col}}{\dfrac{1}{G_{col} - G_{HA}} + \dfrac{6\Phi_{HA}(k_{HA} + 2G_{HA})}{5G_{HA}(3k_{HA} + 4G_{HA})}},$$

Accordingly, Hashin-Shtrikman lower and upper bounds on bone elastic modulus can be obtained as

$$E_{H-S}^{lower} = \frac{9k_{H-S}^{lower} G_{H-S}^{lower}}{3k_{H-S}^{lower} + G_{H-S}^{lower}}, \quad E_{H-S}^{upper} = \frac{9k_{H-S}^{upper} G_{H-S}^{upper}}{3k_{H-S}^{upper} + G_{H-S}^{upper}}. \tag{6.4}$$

Walpole (1966a,b) derived bounds on the elastic moduli of a transversely isotropic composite reinforced with aligned ellipsoidal inclusions with finite length. Such geometry resembles bone more closely than Voigt, Reuss, and Hashin-Shtrikman models. Also, Hill (1964) provided bounds for elastic moduli of transversely isotropic composite containing continuous and perfectly aligned cylindrical fibers. Comparison between the results of Voigt, Reuss, Hashin-Shtrikman, and Hill models for elastic modulus of bone is illustrated in Figure 4.1.

Voigt and Reuss models provide bounds, respectively, on longitudinal and transverse elastic moduli of a composite. Hirsch (1962) linearly combined Voigt and Reuss models to obtain the intermediate properties of a composite. Piekarski (1973) applied Hirsch model to bone and determined its longitudinal elastic modulus as

$$\frac{1}{E_l} = x\left(\frac{1}{\Phi_{col}E_{\text{col}} + \Phi_{HA}E_{HA}}\right) + (1-x)\left(\frac{\Phi_{\text{col}}}{E_{\text{col}}} + \frac{\Phi_{HA}}{E_{HA}}\right), \tag{6.5}$$

where x and $1-x$ are the relative proportion of material conforming with the upper and lower bounds, and x is equal to 0.925, indicating that bone deformation occurs dominantly under uniform strain. Currey (1969) proposed a variant on Voigt model including a reinforcement parameter which accounts for the geometry of fibers as well as the mechanical properties of both matrix and fibers. The effective longitudinal modulus was expressed as

$$E_l = \Phi_{\text{col}}E_{\text{col}} + \Phi_{HA}E_{HA}\left(1 - \frac{2}{\beta L}\right)\tanh\left(\frac{2}{\beta L}\right), \tag{6.6}$$

with

$$\beta = \sqrt{\frac{(2\pi)\,G_{\text{col}}}{E_{HA}A_{HA}\ln\left(\frac{a}{a_{HA}}\right)}}, \tag{6.7}$$

where L, A_{HA}, and a_{HA} are the length, cross-sectional area, and the radius of hydroxyapatite crystals, respectively, and a is the mean separation distance between neighboring crystals.

6.2 Modeling of bone at nanoscale

6.2.1 Models based on strength of materials

Jaeger and Fratzl (2000) proposed a model with a staggered arrangement of hydroxyapatite crystals distributed unequally in the gap and overlap zone of collagen fibrils, as shown in Figure 6.1. In this model, hydroxyapatite crystals carry most of

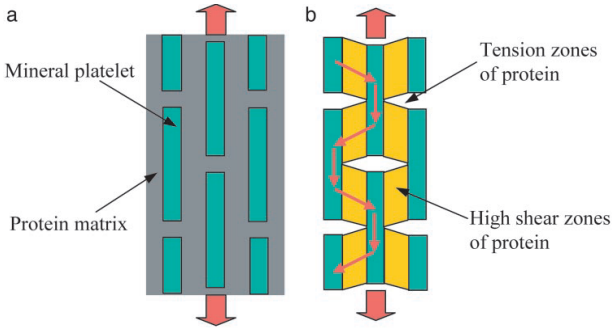

Figure 6.1: A schematic of the shear lag model proposed by Jager and Fratzl (Jager and Fratzl, 2000) representing (a) staggered hydroxyapatite crystals embedded in protein matrix, and (b) the load-carrying structure of the collagen-hydroxyapatite composite (Gao et al., 2003).

the axial stresses, while the collagen matrix transfers stresses between the adjacent platelets via shear. This shear lag model was the basis for most of FEM models proposed later. Using this model, Gao et al. (2003) predicted bone longitudinal elastic modulus to be

$$\frac{1}{E_l} = \frac{4(1-\Phi_{HA})}{G_{col}\Phi_{HA}^2\rho^2} + \frac{1}{\Phi_{HA}E_{HA}}, \tag{6.8}$$

where ρ is the ratio of platelet length to thickness.

Kotha and Guzelsu (2000) extended the shear lag model to investigate the effect of collagen-hydroxyapatite interphase/bonding on mechanical properties of a mineralized fibril. They added a fictitious platelet, with the mechanical properties of an interphase, to the ends of the hydroxyapatite platelets and evaluated the longitudinal elastic modulus of the mineral-organic composite for different values of interfacial modulus.

6.2.2 Models based on micromechanics

Mori-Tanaka (1973) method (MT) was proposed to model non-dilute composite materials. Benveniste (1987) provided a particularly clear explanation of the Mori-

Tanaka theory for two-phase composites with aligned or randomly oriented ellipsoidal particles. Given the stiffness tensors of the matrix, $\mathbf{C}_m$, and the aligned fibers, $\mathbf{C}_f$, the effective stiffness tensor of the composite, $\mathbf{C}$, is

$$\mathbf{C} = \mathbf{C}_m + \Phi_f(\mathbf{C}_f - \mathbf{C}_m)[\mathbf{I} + \mathbf{S}\mathbf{C}_m^{-1}(\mathbf{C}_f - \mathbf{C}_m)]^{-1}$$

$$[(1-\Phi_f)\mathbf{I} + \Phi_f[\mathbf{I} + \mathbf{S}\mathbf{C}_m^{-1}(\mathbf{C}_f - \mathbf{C}_m)]^{-1}]^{-1}, \tag{6.9}$$

where $\mathbf{I}$ is the identity tensor. The superimposed (-1) denotes the inverse, and the tensor products of the type $\mathbf{S}\mathbf{C}_m^{-1}$ are the inner tensor products.

Self-consistent (SC) method was originally proposed by Hershey (1954) and Kroner (1958) for polycrystalline aggregates but developed for composite materials by Hill (1963) and Budiansky (1965). This method assumes a basic element of a heterogeneous medium, such as an inclusion in a particulate composite, to be embedded in an equivalent homogeneous medium with unknown properties. Using this approach, the effective stiffness tensor of the composite is

$$\mathbf{C} = \mathbf{C}_m + \Phi_f(\mathbf{C}_f - \mathbf{C}_m)[\mathbf{I} + \mathbf{S}\mathbf{C}^{-1}(\mathbf{C}_f - \mathbf{C})]^{-1}$$
$$[(1-\Phi_f)\mathbf{I} + \Phi_f[\mathbf{I} + \mathbf{S}\mathbf{C}^{-1}(\mathbf{C}_f - \mathbf{C})]^{-1}]^{-1}. \tag{6.10}$$

Note that Eq.(6.10) is an implicit equation in terms of the unknown $\mathbf{C}$.

MT and SC methods were not originally proposed for modeling of bone. However, later, many researchers used these micromechanical methods to model bone at nanoscale as a collagen-hydroxyapatite composite.

Akkus (2005) developed an inclusion-based micromechanics method to model a mineralized collagen fibril in accordance with the geometry proposed by Fratzl et al. (1991). In this representation, hydroxyapatite crystals are distributed randomly in the transverse plane. Akkus (2005) predicted the effective stiffness of collagen-hydroxyapatite composite as

$$\mathbf{C} = [\mathbf{C}_{col}^{-1} - \Phi_{HA}\{(\mathbf{C}_{HA} - \mathbf{C}_{col})[\mathbf{S} - \Phi_{HA}(\mathbf{S} - \mathbf{I})]$$
$$+\mathbf{C}_{col}\}^{-1}(\mathbf{C}_{HA} - \mathbf{C}_{col})\mathbf{C}_{col}^{-1}]^{-1}. \tag{6.11}$$

Most of the models proposed for modeling of bone at nanoscale only account for collagen and hydroxyapatite. However, recently some researchers proposed micromechanical models accounting for all the components existing in bone, by considering the hierarchical structure of bone at nano and higher scales. Almost all the micromechanics-based models of bone considered collagen as a matrix and hydroxyapatite crystals as reinforcing inclusions. However, Hellmich et al. (2004) considered three different representations for the collagen-mineral interaction, which are shown in Figure 6.2, and used different micromechanical methods to obtain the effective elastic properties of bone at nanoscale. Also, Fritsch and Hellmich (2007) proposed a model for hierarchical organization of bone material in the framework of a multi-step homogenization scheme. They modeled bone at nano and submicroscales by using five steps which are tabulated in Table 6.1.

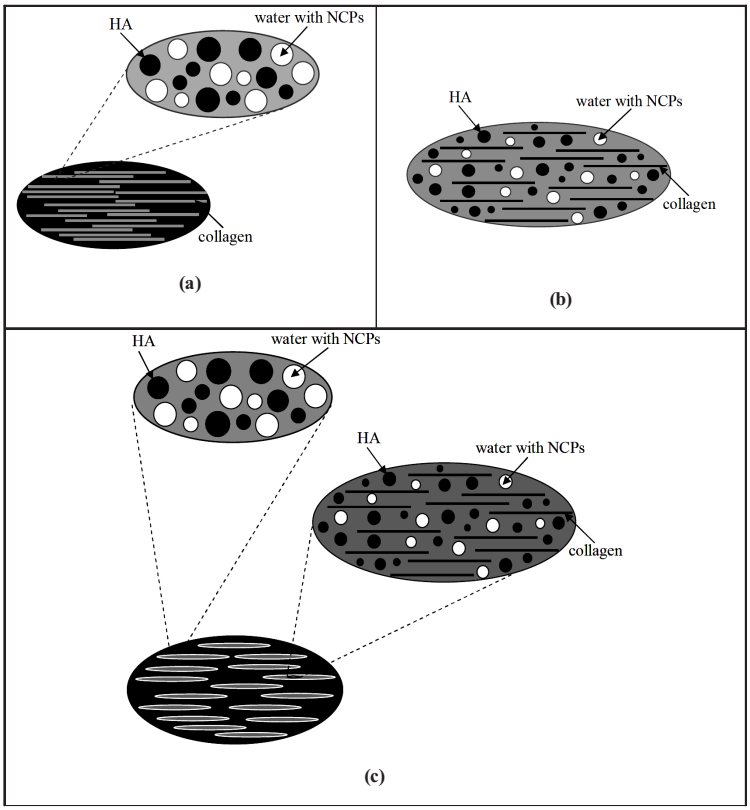

Figure 6.2: Different representations for collagen-mineral interaction in bone (Hellmich et al., 2004): (a) collagen molecules embedded in the hydroxyapatite (HA) foam matrix, (b) interpenetrating network of collagen molecules, HA crystals, and water with non-collagenous proteins (NCPs), and (c) mineralized collagen fibrils embedded in HA foam.

Nikolov and Raabe (2008) estimated the elastic properties of bone at nanoscale via a step-by-step homogenization from the staggered arrangement of collagen molecules up to an array of parallel mineralized fibrils. They proposed a model for extrafibrillar mineralization, assuming that the extrafibrillar minerals are equivalent to reinforcing rings coating each individual fibril. The homogenization steps used in this model are listed in Table 6.2. Also, Yoon and Cowin (2008) predicted the elastic constants of bone at three different hierarchical levels: a mineralized collagen fibril, a mineralized collagen fiber, and a single lamella.

Table 6.1: Hierarchical model of bone at nano and sub-microscales based on a model proposed by Fritsch and Hellmich (2007).

Modeling step	Homogenization procedure	Micromechanics method
I Wet collagen	Continuous collagen matrix perforated by holes containing water and non - collagenous proteins	Mori-Tanaka
II Mineralized collagen fibril	Wet collagen matrix reinforced with spherical hydroxyapatite inclusions	Self-consistent
III Hydroxyapatite foam	Hydroxyapatite crystals and intercrystalline pores interpenetrating each other	Self-consistent
IV Extracellular bone matrix	Mineralized collagen fibrils embedded in the hydroxyapatite foam	Mori-Tanaka
V Single lamella	Lacunae embedded in the extracellular bone matrix	Mori-Tanaka

Finally, Hamed et al. (2010) proposed a multiscale model to evaluate the elastic properties of cortical bone. The model was a bottom-up procedure starting at nanoscale and moving up to sub-microscale, microscale, and mesoscale. Figure 6.3 illustrates the homogenization steps used in this model.

6.2.3 Computational models using finite element modeling (FEM)

Ji and Gao (2006) used the shear lag geometry (Jager and Fratzl, 2000) together with FEM analysis to obtain the anisotropic elastic properties of nanocomposite structure of bone. Siegmund et al. (2008) improved the model by considering the effect of collagen cross-linking and collagen-hydroxyapatite interphase on mechanical behavior of a mineralized collagen fibril. Collagen cross-linking significantly

Table 6.2: Hierarchical model of bone at nanostructural level based on a model proposed by Nikolov-Raabe (2008).

Modeling step	Homogenization procedure	Micromechanics method
I Collagen-water composite	Cylindrical collagen fibers embedded in an isotropic water/non-collagenous protein matrix	Torquato (1998) and Hill's (1964) lower bound
II Mineralized collagen fibril	Collagen-water matrix reinforced with interfibrillar ellipsoidal hydroxyapatite crystals	Mori-Tanaka (1973)
III Mineralized collagen fibrils with extrafibrillar hydroxyapatite	Mineralized collagen fibril coated with an extrafibrillar hydroxyapatite layer	Mori-Tanaka (1973)
IV Bundle of aligned mineralized fibrils	The matrix of step III containing needlelike spaces filled with non - collagenous proteins	Mori-Tanaka (1973)

Table 6.3: Hierarchical model of bone at nano and sub-microscales based on a model proposed by Yoon-Cowin (2008).

Modeling step	Homogenization procedure	Micromechanics method
I Collagen/hydroxyapatite-water composite	Collagen/hydroxyapatite together with bound water	Averaging Voigt and Reuss bounds
II Mineralized collagen fibril	Hydroxyapatite crystals distributed periodically about the long axes of collagen molecules	Platelet shaped composite models (Nemat-Nasser et al., 1982; Nemat-Nasser and Hori, 1999)
III Mineralized collagen fiber	Cylindrical fibrils of step II embedded in hydroxyapatite-water composite	Cylindrical shaped composite models (Nemat-Nasser and Hori,1999)
IV Single lamella	Cylindrical fibers of step III embedded in hydroxyapatite-water composite	Cylindrical shaped composite models (Nemat-Nasser Hori, 1999)

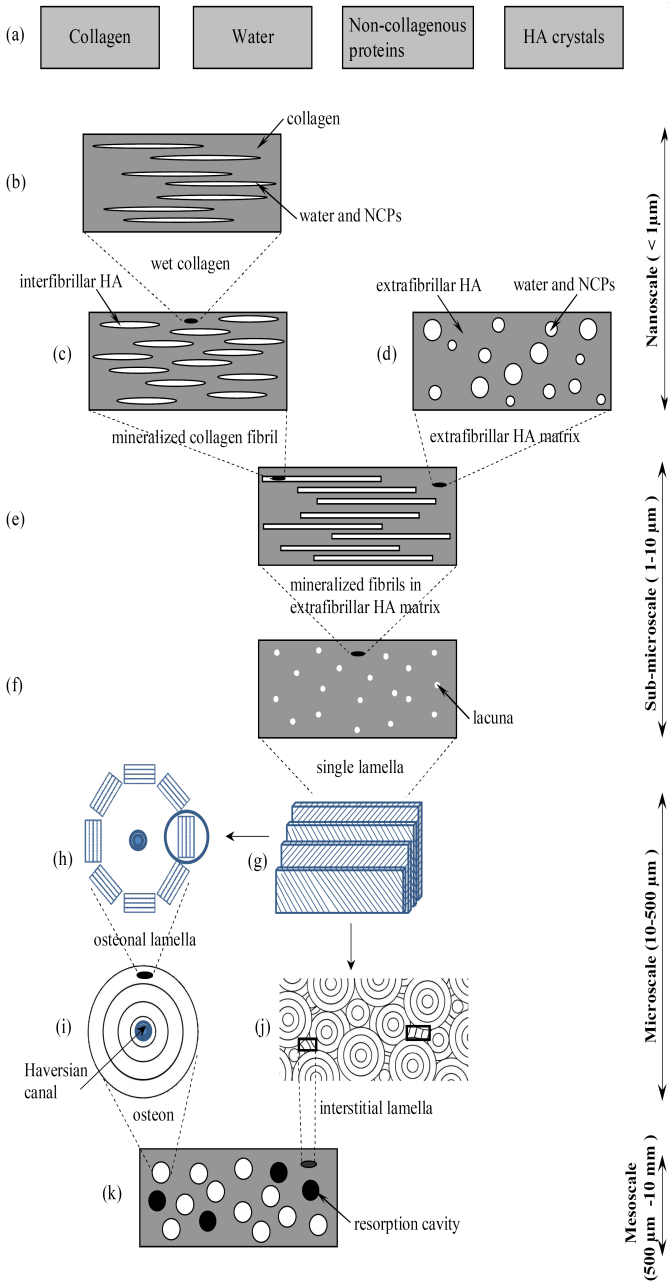

Figure 6.3: Successive homogenization steps in modeling the elastic properties of cortical bone proposed by Hamed et al. (2010).

affects the deformation and failure behavior of bone. An increase in cross-linking improves bone strength and stiffness, while reduces its energy absorption and ductility. In their model, Jager and Fratzl obtained the stress-strain curves of fibrils without any cross-links, with enzymatic cross-links, and with non-enzymatic cross-links. Cross-links were modeled by using cohesive elements at collagen interfaces. The results showed that the enzymatic cross-links have negligible effect on the predicted stress–strain curve and produce a ductile material that fails through debonding of the collagen-hydroxyapatite interface. On the other hand, non-enzymatic cross-links significantly alter the stress–strain response by inhibiting collagen sliding leading to greater load transfer to minerals which, in turn, increases modulus and decreases post-yield strain and toughness. Ghanbari and Naghdabadi (2009) considered bone as a nanocomposite consisting of collagen, mineral, and an interphase layer in between them, and used nonlinear FEM to capture the transversely isotropic behavior of the structure. Yuan et al. (2011) represented the structure of a mineralized collagen fibril both in 2D and 3D and calculated its elastic properties using FEM analysis. The shear lag model (Jager and Fratzl, 2000) was a starting point in this model to develop an improved model incorporating more structural features of the mineralized collagen fibril. They assumed the mineral phase to be rigid with no deformation in comparison with the very soft collagen phase which gave rise to the overestimation of results for elastic modulus of a fibril. Yuan et al. (2011) used the same 2D model with more correct properties of phases to show that the distribution of axial stress/strain or shear stress/strain cannot be neatly partitioned and linearly added. They also extended their FEM analysis to a 3D geometry which is shown in Figure 6.4.

6.2.4 Atomistic simulations using molecular dynamics (MD)

Collagen is the main structural protein of bone. That is the reason why several atomistic simulations were done on tropocollagen. Lorenzo and Caffarena (2005) performed steered molecular dynamics (SMD) simulations to obtain the mechanical properties of collagen. To this end, a collagen-like peptide was solvated in water and equilibrated under the temperature T = 300 K and pressure p = 1 atm. After equilibrium, a fictitious spring was attached to the center of mass of N-terminal atoms and was pulled at a constant velocity along the longitudinal molecular axis. The collagen modulus was found to be 4.8 ± 1.0 GPa. Similarly, Veld and Stevens (2006) did MD simulations on a synthetic peptide representing collagen. The protein was solvated in an aqueous saline solution and was pulled along its molecular axis by moving the terminal residues at constant velocity. The elastic modulus of collagen molecule was 6.1 GPa. Using molecular dynamics, Buehler (2006) studied the mechanical properties of triple-helical collagen-like molecules under different types of loading, including tension, compression, shear, and bending. The simulations were conducted using two types of force fields: classical CHARMM (Mackerell, 1998) and reactive ReaxFF (van Duin, 2001). In the classical force fields the bonds

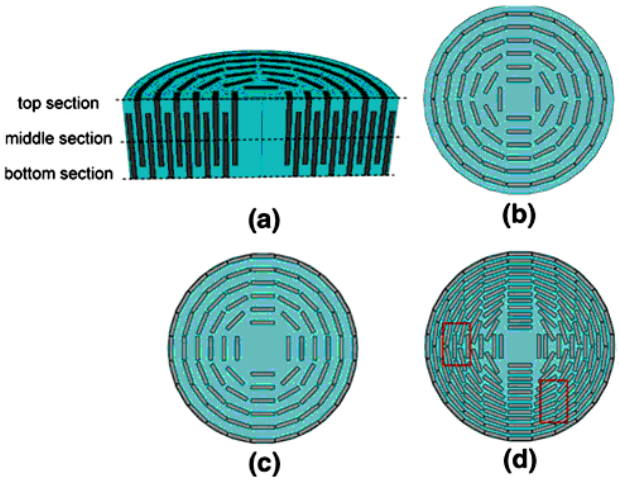

Figure 6.4: 3D FEM model of a cylindrical mineralized collagen fibril (Yuan et al., 2011) representing (a) half-cut view of the fibril showing the staggered pattern of HA crystals which can be divided into (b) top, (c) bottom, and (d) middle sections of the mineralized collagen fibril.

between atoms cannot be broken and new bonds cannot be formed. Reactive force fields, however, can overcome these limitations. Figure 6.5 from Buehler (2006) shows the force-displacement behavior of a collagen molecule under uniaxial tension by using both force fields. Elastic modulus of the collagen molecule was found to be 6.99GPa, 8.71GPa, and 18.82GPa for the loading rates 0.0001 A^o/step, 0.0002 A^o/step, and 0.001 A^o/step, respectively. These results indicate that collagen has a rate-dependent elastic response. Buehler (2008) also used atomistic simulations to assess the effect of cross-linking on the behavior of fibrillar collagen.

As an extension to modeling of collagen, Buehler (2007) modeled a 2D system of a collagen fibril whose gap zones were filled with nano-sized hydroxyapatite crystals, as illustrated schematically in Figure 6.6. The analysis of such a collagen-hydroxyapatite composite revealed that the elastic modulus, yield strength, and fracture strength of mineralized collagen fibril are higher compared to those of pure collagen fibril. Bhowmik et al. (2007) studied the load carrying behavior of collagen in the proximity of hydroxyapatite by pulling a triple-helical collagen molecule, with non-helical ends, both in close proximity and in absence of hydroxyapatite crystals. It was observed that the load-deformation response of solvated collagen in close proximity of HA has features which result from breaking of hydrogen bonds between collagen and water, where water is interacting significantly with hydroxyapatite. Similarly, Dubey and Tomar (2008) studied the collagen-hydroxyapatite

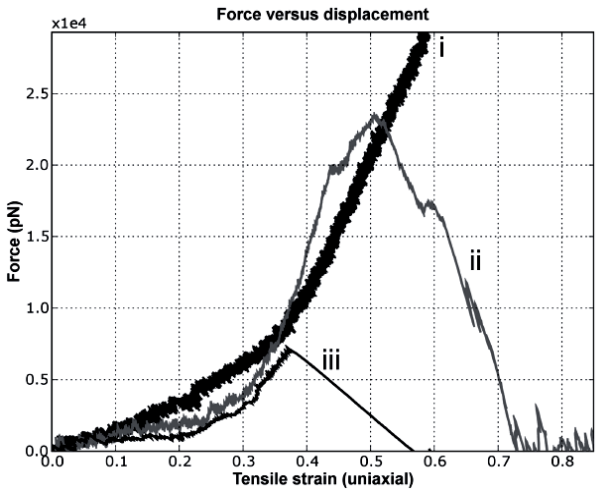

Figure 6.5: MD results of force versus strain for a collagen molecule using (i) nonreactive (CHARMM) and (ii) reactive (ReaxFF) force fields (Buehler, 2006). Curve (iii) depicts the results for stretching of a single polypeptide.

Figure 6.6: The schematic illustration of (a) pure collagen fibril and (b) mineralized collagen fibril with the hydroxyapatite platelets deposited in the gaps (Buehler, 2007).

interface by placing tropocollagen molecules and hydroxyapatite crystals geometrically next to each other and conducting SMD simulations. Comparison between the stress-strain curves of collagen-hydroxyapatite system and pure hydroxyapatite crystals (Figure 6.7) showed that the presence of collagen increases the toughness of hydroxyapatite, while the presence of hydroxyapatite increases the strength of collagen.

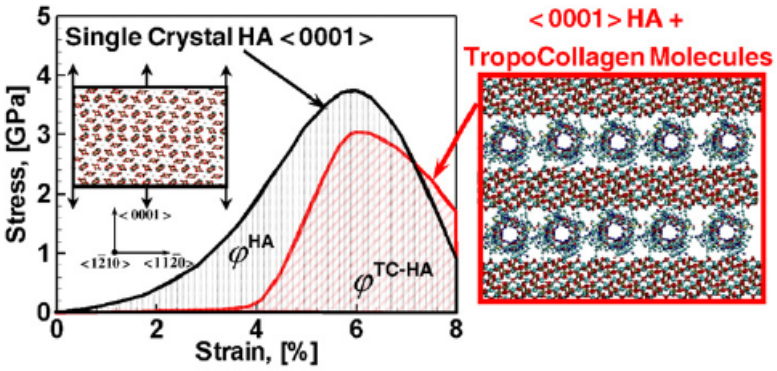

Figure 6.7: Stress-strain curves for a single hydroxyapatite cell and a cell corresponding to the collagen-HA composite (Dubey and Tomar, 2008).

6.3 Modeling of bone at the sub-micron scale

Single lamella consists of preferentially oriented mineralized collagen fibrils containing osteocyte-filled lacunae. As mentioned earlier, some researchers extended their models of bone at nanoscale to sub-microscale and also higher scales. For example Fritsch and Hellmich (2007), Yoon and Cowin (2008), and Hamed et al. (2010) modeled a single lamella analytically by using micromechanics matrix-inclusion theories. Akiva et al. (1998) assumed single lamella to be composed of an array of mineralized collagen fibrils, aligned not only along their fibril axes, but also in terms of their crystal layers. They modeled a single lamella as a platelet-reinforced composite and evaluated its orthotropic elastic constants. Jasiuk and Ostoja-Starzewski (2006) modeled a single lamella as a spatially random network of mineralized collagen fibrils and computed its effective anisotropic stiffness tensor by using FEM analysis. The later model did not account for a background material to connect the fibrils to each other but allowed for the connection of fibrils through their intersections.

6.4 Modeling of bone at the microscale

Single lamellae are oriented in different orientations to build the lamellar structures of bone: a single osteon in cortical bone and a single trabecula in trabecular bone. Several types of fibril orientations were reported in literature including orthogonal and twisted plywood patterns (Giraud-Guille, 1988). In the twisted plywood motif there is a fixed angle of orientation between neighboring lamellae and there is also a rotation along the longitudinal axis, while in the orthogonal pattern the angle between the adjacent layers differs by 90 degrees. Figure 6.8 (Martin et al., 1998) shows the twisted plywood structure schematically. Here, we review the existing models of bone at microscale separately for cortical and trabecular bone types.

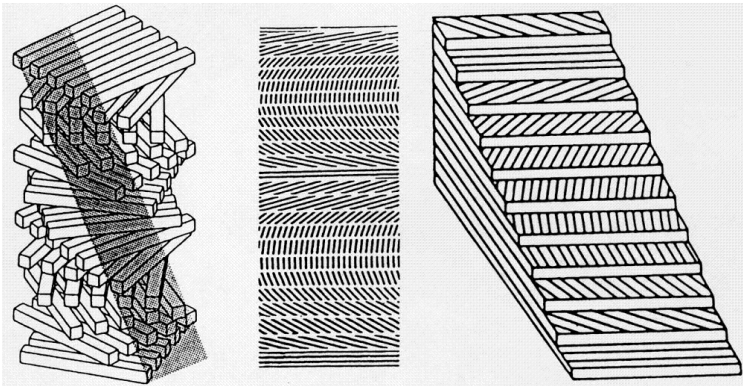

Figure 6.8: Twisted plywood pattern of collagen fibrils in lamellar structures of bone (Martin et al., 1998).

6.4.1 Modeling of cortical bone

Aoubiza et al. (1996) modeled an osteon as a set of concentric lamellae. To this end, they divided the osteonal lamellae and osteon into cylindrical sectors, each sector being approximated as a parallelepiped having a periodic structure. The osteonal lamella was modeled by a superimposition of plates with a periodic structure. Akiva et al. (1998) modeled the lamellar structure of bone by assuming that the lamellar unit is composed of stacked sets of ordered lamellae comprising a thin lamella, a transition zone, a thick lamella, and a 120^o back-flip lamella. After calculating the orthotropic elastic moduli of each of these lamellar parts, they were rotated in space in accordance with the rotated plywood model, and then were stacked together to present the overall elastic behavior of lamellar bone. Dong and Guo (2006) represented an osteon as a two-phase composite with the Haversian canals as inclusions and the surrounding osteonal lamellae as matrix, Figure 6.9

(level 1). They used generalized self-consistent method to evaluate the effective

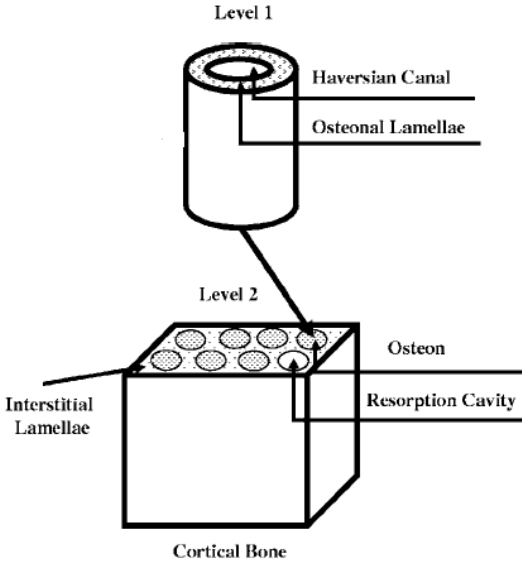

Figure 6.9: A two-level micromechanical model of cortical bone: (level 1) modeling of an osteon, and (level 2) modeling of cortical bone as a collection of osteons and resorption cavities in the interstitial lamellae (Dong and Guo, 2006).

elastic properties of an osteon. Both Haversian canals and osteonal lamellae were assumed to be transversely isotropic with their elastic properties taken from literature. Hamed et al. (2010) followed the same procedure to model an osteon. However, instead of taking the properties of an osteonal lamella from literature, they used laminated composite material theories to calculate the elastic properties of concentric osteonal lamellae, which are composed of single lamellae oriented in a twisted plywood pattern. The homogenization steps used by Hamed et al. to model an osteonal lamella and a single osteon are illustrated in Figures 6.3 (g), (h), and (i).

Aoubiza et al. (1996) represented the interstitial system as a set of homogeneous blocks, each block being a fragment of an old osteon. The properties of an interstitial lamella were then determined by stacking all the blocks. Hamed et al. (2010) modeled an interstitial lamella using the same homogenization procedure they used for an osteonal lamella. The only difference between these two structures is their degree of mineralization (DOM): interstitial lamellae are generally more mineralized and, consequently, stiffer compared to osteonal lamellae. Therefore,

they used a higher DOM while modeling an interstitial lamella.

6.4.2 Modeling of trabecular bone

Trabecular bone tissue properties were mainly studied experimentally using tensile test (Ryan and Williams, 1989; Bini et al., 2002), bending test (Choi and Goldstein, 1992; Tanaka et al., 2010), ultrasound (Rho et al., 1993), and nanoindentation (Rho et al., 1997; Zysset et al., 1998; Brennan et al., 2009). Rice et al. (1988) obtained experimentally elastic modulus of trabecular bone and used that data together with Christensen's (1986) model for low density materials to back-calculate bone's tissue properties. Similarly, 3D FEM models along with experimental data for apparent trabecular modulus were used to back-calculate elastic modulus of trabecular bone tissue (van Rietbergen et al., 1995; Ulrich et al., 1997; van Eijden et al., 2004; Bayraktar et al., 2004). Moreover, Hamed et al. (2011) applied laminated composite material theories to model a single trabecula as an isotropic material formed by randomly oriented single lamellae. Note that all the models used the simplifying assumption of isotropy and homogeneity for a single trabecula which is not the case in reality.

6.5 Modeling of bone at the mesoscale

6.5.1 Modeling of cortical bone

Cortical bone is a collection of osteons, resorption sites, and interstitial lamellae. Hogan (1992) developed a model of cortical bone in which the osteons and interstitial lamellae were considered to be the fiber and matrix, respectively, and the cement line was modeled as an interphase component. FEM analysis was used to obtain the elastic properties of such a cortical bone system. Aoubiza et al. (1996) modeled cortical bone as a composite medium made of hollow fibrous osteons embedded in the interstitial system and used a homogenization theory to obtain its elastic properties. The osteons were assumed to be periodically distributed in the matrix and the cement line was assumed to be a rigid interface. Similarly, Dung and Guo (2006) used the generalized self-consistent method to model a cortical bone with the interstitial lamella being a matrix and osteons together with resorption sites being two types of inclusions, Figure 6.9 (level 2). Hamed et al. (2010) assumed the same matrix-inclusions arrangement, as shown in Figure 6.3(k), but used the hybrid Mori-Tanaka method to obtain the effective elastic constants of cortical bone. Parnell and Grimal (2009) proposed a model of cortical bone to assess the effect of mesoscale porosity, containing Haversian canals and resorption cavities, on the anisotropy of the material. The mesoscale pores were surrounded by an isotropic bony matrix tissue. They derived the input parameters of the model from mesoscale experimental data, such as scanning acoustic microscopy (SAM), and used the method of asymptotic homogenization to determine the local

effective elastic properties of cortical bone. Grimal et al. (2011) proposed a two-parameter macroscale model to predict the effective elastic moduli of cortical bone. They regarded cortical bone as a two-phase composite with a mineralized matrix (ultrastructure) perforated by cylindrical pores (vascular porosity). The two key parameters of this model were the volume fractions of hydroxyapatite and vascular porosity. Table 6.4 lists selected modeling results for longitudinal elastic modulus of cortical bone at micro and mesoscales.

Table 6.4: Selected modeling results for longitudinal elastic modulus of cortical bone at different hierarchical scales.

Tissue	Modeling method	Elastic modulus (GPa)	Reference
Osteonal lamella	Laminated composite materials theories	17.91	Hamed et al. (2010)
Osteonal lamella	Strength of materials models	22.9	Akiva et al. (1998)
Interstitial lamella	Laminated composite materials theories	21.24	Hamed et al. (2010)
Cortical bone	Micromechanics	14.35-17.8	Dong and Guo (2006)
Cortical bone	Micromechanics	17.12	Aoubiza et al. (1996)
Cortical bone	Micromechanics	18.69	Hamed et al. (2010)
Cortical bone	Finite element	18.9-20.4	Hogan (1992)

6.5.2 Modeling of trabecular bone

Trabecular bone is a foam-like structure consisting of a porous network of trabeculae. Gibson and Ashby (1982) and Gibson et al. (1982) developed a theory to predict the elastic modulus of a cellular solid by power law relations in terms of its density, as described in Section 1.

Although trabecular bone apparent density is a key parameter in determining its properties, it alone cannot fully capture bone's mechanical behavior. Trabecular bone architecture, characterized by thickness, number, and separation distance of individual trabecula and their 3D connectivity, plays an important role in its mechanical response. Therefore, high-resolution images, such as micro-CT images,

of trabecular bone samples were used as inputs for FEM analysis to predict elastic moduli of bone based on its actual geometry (van Rietbergen et al., 1995; Muller and Ruegsegger, 1995; Ulrich et al., 1998; Jaasma et al., 2002; Homminga et al., 2003; Bourne and van der Meulen, 2004; Dobson et al., 2006; BeVill et al., 2007; Follet et al., 2007; Chevalier et al., 2007; Harrison et al., 2008; Hamed et al., 2011).

Alternatively, some analyses used idealized periodic geometry of trabecular bone, composed of networks of beams and plates, rather than its actual geometry (Kowalczyk, 2003; Yoo and Jasiuk, 2006; van Lenthe et al., 2006; Donaldson et al., 2008; Ilic et al., 2010). Voronoi techniques were also used to generate a non-periodic mesh representing the trabecular bone (Silva and Gibson, 1997; Ruiz et al., 2010). Figure 6.10 shows examples of different geometries used in elastic modeling of trabecular bone. Table 6.5 gives selected modeling results for elastic modulus of

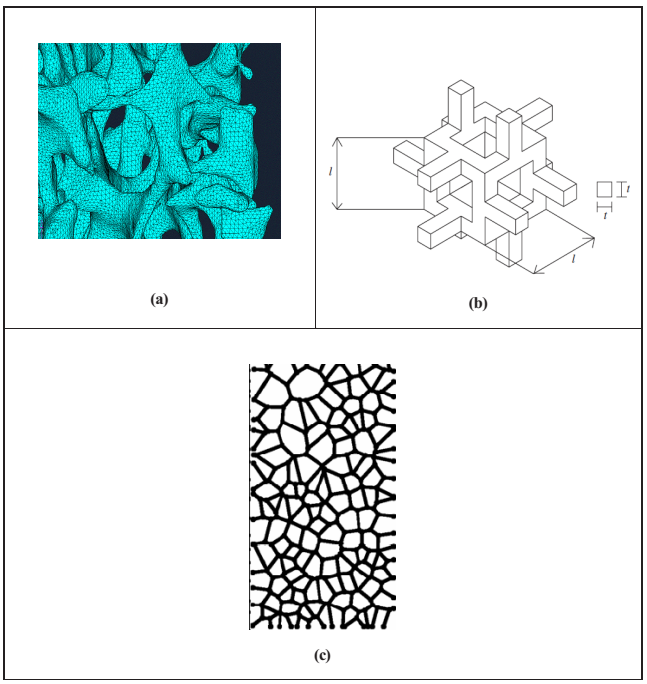

Figure 6.10: Examples of different geometris used in the elastic modeling of trabecular bone: (a) actual 3D geometry obtained by micro-CT (Hamed et al., 2011), (b) a 3D idealized periodic geometry (Yoo and Jasiuk, 2006), (c) a 2D idealized microstructure constructed by Voronoi algorithms (Ruiz et al., 2010).

trabecular bone at micro and mesoscales.

Table 6.5: Selected modeling results for elastic modulus of trabecular bone at different hierarchical scales.

Tissue	Modeling method	Young's modulus (GPa)	Reference
Single trabecula	Experiment-FEM	2.23-10.1	van Rietbergen et al. (1995)
Single trabecula	Experiment-FEM	3.5-8.6	Ulrich et al. (1997)
Single trabecula	Experiment-FEM	11.87±2.74	Van Eijden et al. (2004)
Single trabecula	Laminated composite materials theories	7.84-20.24	Hamed et al. (2011)
Single trabecula	Experiment-FEM	18.0±2.8	Bayraktar et al. (2004)
Trabecular bone	lattice-based FEM	0.161-0.444	Diamant et al. (2005)
Trabecular bone	μCT-based FEM	1.64±0.32	Harrison et al. (2008)

7 Discussion

From an experimental point of view, careful attention should be paid to bone storage and preparation. Basic measurements should be performed on samples to determine the water, mineral, and protein fractions, as well as the density and porosity. The samples should be tested in the hydrated condition.

The type of bone and location of the specimen must also be reported. Elastic moduli are typically reported for long bones (femur, tibia, etc.), but ribs, skull bones and vertebra moduli have also been reported. The location of the sample is equally important. For example, 'femur bone' has a wide variety of bone microstructural configurations, depending on the location. The age of the bone should also be reported. Many data are taken on bovine femur bone because of its wide availability. Cattle are typically slaughtered at $\sim$ 18 months age, so that most 'grocery store'

bone is of that age. Also, there is a wide variability in the degree of mineralization in human bone as a function of age, which is strongly correlated with the elastic modulus.

The orientation of the samples is of utmost importance. Femoral cortical bone is transversely isotropic – properties in longitudinal direction are significantly different than those in the transverse direction. Care needs to be taken to cut samples so that one or the other orientation is tested. This also applies to trabecular bone, which at first glance may look isotropic, but is actually anisotropic.

Bulk mechanical (tension, compression, flexure) test conditions must also be reported. Bone is strain rate sensitive and the deformation rate needs to be given. Typically, under quasi-static tests (10^{-2} - 10^{-4}/sec), the strain-rate effect is not significant, but at higher strain rates, the elastic modulus becomes larger. Knowledge of bone mechanical behavior for different strain rates is particularly important for sport medicine since traumatic bone failure usually occurs at the high strain rates. Unless the geometric configuration is given, plots of force/displacement curves should be avoided.

Nanoindentation (instrumented with a diamond tip or from atomic force microscopy) recently opened the new horizons in the field of bone characterization. These techniques are extremely powerful because they allow measurement of the elastic moduli of individual microstructural constituents such as osteons and interstitial lamellae. Moreover it is possible to investigate properties in physiological conditions: from ambient environment to submerged in physiological buffered solutions. In addition, other important mechanical properties such as the viscoelastic response can be evaluated. It should be kept in mind that indentation techniques measure the properties in a very small region close to the surface and do not represent the 'bulk properties.' The elastic modulus measured by nanoindentation is typically larger than bulk measurements, since the effect of porosity is not detected for such a small probed area. However, the surface properties can be extremely useful for the evaluation of bone tissue response to implants and other bone substitutes.

Microindentation has been applied to a novel test method to probe bone quality *in vivo* (Hansma et al., 2006, 2008). The utilized medical instrument is less invasive than in other methods and permits careful choice of the location and force of the indentation.

A summary of the important parameters that affect the measurement of the elastic modulus of bone is given in Table 7.1, demonstrating that mechanical tests of bone are not as straightforward as testings of traditional engineering materials.

Correlation of the mechanical properties with the structure of bone can be performed at all hierarchical levels (Figure 3.1). Standard methods such as optical microscopy and electron microscopy are routinely reported in the literature and yield insight into the basic organization. Confocal microscopy and computed tomography have been recently applied to evaluate bone architecture and have

Table 7.1: Summary of the important parameters that affect the measurement of the elastic modulus of bone.

Parameter	Explanation	Effect
Bone type	Trabecular, cortical, woven	Widely varying values (between 8.4 GPa for dolphin rib and 34.1 GPa for whale bulla (Currey, 2010).
Location	Femur, skull, tibia, rib, radius, ulna, antler, bulla	Widely varying values depending on biological adaptation of the particular bone (Currey, 1990, 2010).
Taxa	Human, bovine, reptile, bird	Proportionally higher for larger animals (Currey, 1990; Erickson et al., 2002).
Hydration	Wet collagen fibers contribute to the whole bone mechanical response	Hydration decreases elastic modulus.
Age	(a) Bone mineralization is progressively increasing until the full maturity, and after that starting to decrease. (b) Changes in collagen cross-linking at nanoscale and increasing the density of secondary osteons with age	(a) Elastic modulus progressively increased until full maturity (Currey et al., 1996), and started to decrease because of bone demineralization process. (b) Fracture receptivity is increasing with age (Ritchie et al., 2006; Nalla et al., 2006).
Strain rate	Elastic modulus is different for quasi-static and dymnamic tests	Increasing strain rate increases elastic modulus (Zioupos et al., 2008; Hansen et al., 2008; Kulin et al., 2011).
Location along the same bone	Elastic modulus is slightly different for femur neck, femur midshaft, femur head.	Different for different location along the same bone, depending on bone biological adaptation (Thurner, 2009).

emerged as strongly effective methods to visualize the three-dimensional structure. In particular, CT results can be used as inputs for theoretical or computational models.

We reviewed a number of analytical and computational modeling techniques for predicting the elastic properties of bone at different scales. Several simplifying assumptions and selections were made in all models. Even the classification of scales is not unique or fixed. The transition between different hierarchies in real bone, from nanoscale to macroscale, is continuous rather than discrete. However, in modeling, one can account for a limited number of length scales. Also, for simplicity, the models used the assumption about the separation of scales and the existence of a representative volume element at each scale, implying that bone features at the previous scale are much smaller compared to those at the next scale. However, in bone, the features at a previous scale might be comparable to a larger scale.

A challenging issue in modeling of bone is the selection of mechanical properties and volume fractions of the constituents in bone. There is a wide range of values in literature for the elastic moduli of collagen and hydroxyapatite crystals, see (Hamed et al., 2010), while no data is available for the mechanical properties of NCPs. Different choices for such properties may result in very different outcomes. Moreover, the behavior and mechanical properties of collagen cross-links and collagen-hydroxyapatite interphase are still open to question. Kotha and Guzelsu (2000) as well as Ghanbari and Naghdabadi (2009) assessed the effect of collagen-hydroxyapatite interphase on the elastic properties of bone at nanoscale. Kotha and Guzelsu (2000) selected the elastic modulus of collagen to be 2.7 GPa and tried different values of 0.135, 0.675, and 2.7 GPa for interfacial modulus. On the other hand, Ghanbari and Naghdabadi (2009) chose the elastic modulus of collagen and interphase to be, respectively, 0.2 GPa and 7 GPa. These two very different selections of material properties show the necessity of experimental characterization of the properties of bone components at nanoscale. Also, experimental measurements of collagen elastic modulus are highly dependent on the dehydration state of the specimen. Several studies confirmed a significant increase in collagen elastic modulus upon dehydration (Cusack and Miller, 1979; van der Rijt et al., 2006; Yang et al., 2007). However, not many of the existing modeling techniques can capture such a trend. Finally, most of the models assumed collagen, hydroxyapatite, and NCPs to be linear elastic and isotropic. A more realistic model should account for viscoelastic, nonlinear and anisotropic behavior of collagen and NCPs.

Most of the models made simplifications to the actual geometries and microstructures of bone at different scales. As an illustration, while modeling a single lamella, the existing models assumed that parallel layering of hydroxyapatite crystals in a collagen fibril is aligned with crystal layers in adjacent fibrils (Weiner and Traub, 1992; Erts et al., 1994). However, some studies suggested that crystals have a random arrangement rather than an orderly alignment in neighboring collagen fibrils (Glimcher, 1984; Rubin et al., 2003). Another issue is the orientation pat-

tern of lamellae in lamellar structures of bone. Several models adopted the twisted plywood pattern, while others used the orthogonal plywood motif. The orthogonal and twisted plywood models predict different elastic symmetries for the lamellar structures of bone: orthogonal plywood has orthotropic elastic symmetry, while the twisted plywood does not (Turner et al., 1995). Even in the twisted architecture of collagen fibrils, there is not a consensus on the degree of rotation between successive lamellae. Weiner et al. (1997) found that there is a bimodal peak at 30° and 70° in the collagen fibril arrays suggesting that the angle changes in increments of 30°, from 0° to 120° and then back to 0° again. Hamed et al. (2010) used a complete 180° turning with increments of 30°. If the lamellae do not complete a 180° turning, an in-plane isotropic response could not be obtained. Another phenomenon is the variation of degree of mineralization in different lamellae. Some experiments confirmed that, in cortical bone, the DOM decreases from the interior part of the osteon to the middle part and then increases again until reaching the cement line (Timlin et al., 1999). Such a variation in DOM could change the elastic properties across the lamellae. However, most of the models assumed a constant value of DOM for all lamellae instead of a gradient one. Similar issue holds for trabecular bone. Several studies showed that elastic properties of trabecular bone at microscale change across thickness of a single trabecula (van der Linden et al., 2004; Harrison et al., 2008) with a trend of gradual reduction in tissue modulus from center to surface of trabeculae, where older bone at strut interior is more mineralized compared to the newly formed bone at strut surface.

Various studies have used different analytical and computational models to evaluate the elastic constants of bone. Yet, those selections are not unique and other modeling techniques could be used alternatively. Micromechanics matrix-inclusion methods, with collagen being a matrix and hydroxyapatite crystals being inclusions, were among the most popular models. However, a recent study on completely deproteinized trabecular bone showed that minerals form a continuum phase in bone (Chen et al., 2011), in which both collagen and hydroxyapatite intertwine each other. Therefore, interpenetrating theories, like SC method (with no matrix), are better candidates to obtain the elastic properties of bone at nanoscale compared to matrix-inclusion theories, like MT method.

8 Conclusions

A number of analytical and computational modeling techniques for predicting the elastic properties of bone at different scales were reviewed along with several important experimental techniques. It was shown that sophisticated hierarchical structure of bone makes the modeling of a mechanical response of bone extremely challenging. Our major findings and conclusions are:

- Bone is a complex, hierarchical, anisotropic composite material that has properties that are dependent on a number of variables.

- Experimental values for elastic modulus of bone are highly dependent on mineralization, porosity, location, taxa, density, age, hydration, strain rate, sample size and the testing method.
- Experimental evaluation of the elastic modulus showed the wide range of the values, even for one particular bone (femur in this review).
- Nanoindentation is a new method that can be used to probe individual microstructural features. Reported elastic moduli are higher than those from bulk measurements.
- Microindentation opens the new horizons for the evaluation of bone material properties *in vivo.*
- Micro- and nano-computed tomography are extremely powerful methods of evaluation of bone internal structure.
- All the modeling techniques use simplifying assumptions about the inputs including the geometries and microstructures of bone, as well as the mechanical properties and volume fractions of different constituents.
- To obtain the structure-property relations in bone, there is a need to generate models with inputs obtained experimentally. As an example, micro-CT imaging has enabled obtaining the actual 3D geometry of bone, which can be used as an input for FEM models.
- At the nanoscale, there are still many uncertainties and open issues. More powerful imaging techniques and testing methods are needed to characterize the geometry and mechanical behavior of a mineralized collagen fibril and to provide data needed in the modeling.

Acknowledgements

UC San Diego group gratefully acknowledges the financial support from the National Science Foundation, Division of Materials Research, Ceramics Program (Grant 1006931). The University of Illinois group gratefully acknowledges the financial support from the National Science Foundation, Civil, Mechanical and Manufacturing Innovation (Grant 09-27909).

References

U. Akiva, H.D. Wagner, S. Weiner, Modelling the three-dimensional elastic constants of parallel-fibred and lamellar bone, J. Mat. Sci., 33, (1998), 1497-1509.

O. Akkus, Elastic deformation of mineralized collagen fibrils: An equivalent

inclusion based composite model, J. Biomech. Eng., 127, (2005), 383-390.

Y.H. An, R.A. Draughn, Mechanical testing of bone and the bone-implant interface, CRC Press, 1999.

B. Aoubiza, J.M. Crolet, A. Meunier, On the mechanical characterization of compact bone structure using homogenization theory, J. Biomech., 29, (1996), 1539-1547.

A.L. Arsenault, Image analysis of mineralized and non-mineralized type I collagen fibrils, J. Electron Microsc. Tech., 18, (1991), 262-268.

M.F. Ashby, On engineering properties of materials, Acta Metall., 37, (1989), 1273-1293.

G. Balooch, M. Balooch, R.K. Nalla, S. Schilling, E.H. Filvaroff, G.W. Marshall, S.J. Marshall, R.O. Ritchie, R. Derynck, T. Allison, TGF-beta regulates the mechanical properties and composition of bone matrix, Proc. Natl. Acad. Sci., 102, (2005) 18813–18818.

M.M. Barak, J.D. Currey, S. Weiner, R. Shahar, Are tensile and compressive Young's moduli of compact bone different? J. Mech. Behav. Biomed. Mater., 2, (2009), 51-60.

A. Basillais, S. Bensamoun, C. Chappard, B. Brunet-Imbault, G. Lemineur, B. Ilharreborde, M.H.B Tho, C.L. Benhamou, Three-dimensional characterization of cortical bone microstructure by microcomputed tomography: validation with ultrasonic and microscopic measurements, J. Orthop. Sci., 12, (2007), 141–148.

H.H. Bayraktar, E.F. Morgan, G.L. Niebur, G.E. Morris, E.K. Wong, T.M. Keaveny, Comparison of the elastic and yield properties of human femoral trabecular and cortical bone tissue, J. Biomech., 37, (2004), 27-35.

H. Beaupied, E. Lespessailles, C.-L. Benhamou, Evaluation of macrostructural bone biomechanics, Joint Bone Spine, 74, (2007), 233-239.

Y. Benveniste, A new approach to the application of Mori-Tanaka theory in composite materials, Mech. Mater., 6, (1987), 147-157.

C. Berthet-Colominas, A. Miller, S.W. White, Structural study of the calcifying collagen in turkey leg tendons, J. Mol. Biol., 134, (1979), 431-445.

G. BeVill, S.K. Easley, T.M. Keaveny, Side-artifact errors in yield strength and elastic modulus for human trabecular bone and their dependence on bone

volume fraction and anatomic site, J. Biomech., 40(15), (2007), 3381-3388.

R. Bhowmik, K.S. Katti, D.R. Katti, Mechanics of molecular collagen is influenced by hydroxyapatite in natural bone, J. Mater. Sci., 42, (2007), 8795-8803.

F. Bini, A. Marinozzi, F. Marinozzi, F. Patane, F., Microtensile measurements of single trabeculae stiffness in human femur, J. Biomech., 35, (2002), 1515-1519.

L.C. Bonar, S. Lees, H.A. Mook, Neutron diffraction studies of collagen in fully mineralized bone, J. Mol. Biol., 181, (1985), 265-270.

W. Bonfield, A.E. Tully, Ultrasonic analysis of the Young's modulus of cortical bone, J. Biomech., 4, (1982), 23-27.

W. Bonfield, E.A. Clark, Elastic deformation of compact bone, J. Mater. Sci., 8, (1973), 1590-1594.

W. Bonfield, M.D. Grynpass, Anisotropy of Young's modulus of bone, Nature, 270, (1977), 453-454.

W. Bonfield, P.K. Datta, Young's modulus of compact bone, J. Biomech., 7, (1974), 147-149.

A.M. Boot, M.A.J. de Ridder, H.A.P. Pols, E.P. Krenning, S.M.P.F. de Muinck Keizer-Schrama, Bone mineral density in children and adolescents: Relation to puberty, calcium intake, and physical activity, J. Clinical Endochrin. Metabol., 82 (1997) 57-62.

A. Boskey, Bone mineral crystal size, Osteoporos. Int., 14 (2003), 16-21.

B.C. Bourne, M.C.H. van der Meulen, Finite element models predict cancellous apparent modulus when tissue modulus is scaled from specimen CT-attenuation, J. Biomech., 37(5), (2004), 613-621.

M.L. Bouxsein, Biomechanics of age-related fractures. In: Osteoporosis, 3rd ed., R. Marcus, D. Feldman, D. Nelson, C.J. Rosen, eds., (2008), Chapter 23, pp. 601–621, Elsevier, Inc.

O. Brennan, O.D. Kennedy, T.C. Lee, S.M. Rackard, F.J. O'Brien, Biomechanical properties across trabeculae from the proximal femur of normal and ovariectomised sheep, J. Biomech., 42, (2009), 498-503.

K. Bruyre Garniera, R. Dumasa, C. Rumelharta, M.E. Arlotb, Mechanical characterization in shear of human femoral cancellous bone: torsion and shear tests, Med. Eng. Phys., 21, (1999), 641-649.

B. Budiansky, On elastic moduli of some heterogeneous materials, J. Mech. and Phys. of Solids, 13(4), (1965), 223-.

M.J. Buehler, Atomistic and continuum modeling of mechanical properties of collagen: Elasticity, fracture, and self-assembly, J. Mater. Res., 21, (2006), 1947-1961.

M.J. Buehler, Molecular nanomechanics of nascent bone: fibrillar toughening by mineralization, Nanotechnology, 18, (2007), art. no. 295102.

M.J. Buehler, Nanomechanics of collagen fibrils under varying cross-link densities: Atomistic and continuum studies, J. Mech. Behav. Biomed. Mater., 1, (2008), 59-67.

H.R. Buie, G.M. Campbell, R.J. Klinck, J.A. MacNeil, S.K. Boyd, Automatic segmentation of cortical and trabecular compartments based on a dual threshold technique for in vivo micro-CT bone analysis, Bone, 41, (2007), 505–515.

A.H. Burstein, J.D. Currey, V. H. Frankel, D.T. Reilly, The ultimate properties of bone tissue: The effects of yielding, J. Biomech., (1972), 5, 35-42.

I.L. Cameron, N.J. Short, G.D. Fullerton, Verification of simple hydration/dehydration methods to characterize multiple water compartments on tendon type I collagen, Cell Biology International, 31, (2007), 531-539.

D.R. Carter, W.C. Hayes, The compressive behavior of bone as a two-phase porous structure, J. Bone Joint Surg. Am., 59, (1977), 954-62.

P.-Y. Chen, D. Toroian, P.A. Price, J. McKittrick, Minerals form a continuum phase in mature cancellous bone, Calcif. Tiss. Inter., 88, (2011), 351-361.

Y. Chevalier, D.H. Pahr, H. Allmer, M. Charlebois, P.K. Zysset, Validation of a voxel-based FE method for prediction of the uniaxial apparent modulus of human trabecular bone using macroscopic mechanical tests and nanoindentation, J. Biomech., 40, (2007), 3333-3340.

K. Choi, S.A. Goldstein, A comparison of the fatigue behavior of human trabecular and cortical bone tisue, J. Biomech., 25, (1992), 1371-1381.

R.M. Christensen, Mechanics of low density materials, J. Mech. Phys. Solids, 34, (1986), 563-578.

S.C. Cowin, S.B. Doty, Tissue Mechanics, Springer, New York, 2007.

S.C. Cowin, Bone mechanics handbook, 2nd Edition, CRC Press, Boca Raton, 2001.

S.C. Cowin, Bone poroelasticity, J. Biomech., 32, (1999), 217-238.

M. Cuppone, B. B. Seedhom, E. Berry, A. E. Ostell, The longitudinal Young's modulus of cortical bone in the midshaft of human femur and its correlation with CT scanning data, Calcif. Tiss. Inter., 74, (2004), 302-309.

J.D. Currey, Bones: Structure and mechanics, Princeton, Princeton University Press, 2002.

J.D. Currey, Effects of differences in mineralization on the mechanical properties of bone, Phil. Trans. Royal Soc. Lond., 304, (1984), 509-518.

J.D. Currey, K. Brear, Hardness, Young's modulus and yield stress in mammalian mineralized tissues, J. Mater. Sci.- Mater. Med., 1, (1990), 14-20.

J.D. Currey, K. Brear, P. Zioupos, The effects of ageing and changes in mineral content in degrading the toughness of human femora, J. Biomech., 29, (1996), 257-260.

J.D. Currey, Mechanical consequences of variation in mineral content of bone, J. Biomech., 2, (1969b), 1-11.

J.D. Currey, Mechanical properties and adaptations of some less familiar bony tissues, J. Mech. Behav. Biomed. Mater., 3, (2010), 357-372.

J.D. Currey, Tensile yield in compact bone is determined by strain, post-yield behaviour by mineral content, J. Biomech., 37, (2004), 549-556.

J.D. Currey, The effect of porosity and mineral content on the Young's modulus of elasticity of compact bone, J. Biomech., 21, (1988a), 131-139.

J.D. Currey, The effects of drying and re-wetting on some mechanical properties of cortical bone, J. Biomech., 21, (1988b), 439-441.

J.D. Currey, The evolution of the mechanical properties of amniote bone, J.Biomech., 20, (1987), 1035-1044.

J.D. Currey, The relationship between the stiffness and the mineral content of bone, J. Biomech., 2, (1969a), 477-480.

J.D. Currey, What determines the bending strength of compact bone? J. Experim. Biol., 202, (1999), 2495-2503.

S. Cusack, A. Miller, Determination of the elastic constants of collagen by Brillouin light scattering, J. Mol. Biol., 135, (1979), 39-51.

C.C. Danielsen, Li. Mosekilde, J. Bollerslev, Le. Mosekilde, Thermal stability of cortical bone collagen in relation to age in normal individuals and in individuals with osteopetrosis, Bone, 15, (1994), 91-96.

J.M. Deuerling, D.J. Rudy, G.L. Niebur, R.K. Roeder, Improved accuracy of cortical bone mineralization measured by polychromatic microcomputed tomography using a novel high mineral density composite calibration phantom, Med. Phys., 37, (2010), 5138-5145.

I. Diamant, R. Shahar, A. Gefen, Predicting apparent elastic moduli of vertebral cancellous bone based on apparent morphology: toward patient-specific spine models, Proc. Bioengineer. Conf., (2005), 33-34.

M. Ding, A. Odgaard, I. Hvid, Accuracy of cancellous bone volume fraction measured by micro-CT scanning, J. Biomech., 32, (1999), 323–326.

C.A. Dobson, G. Sisias, R. Phillips, M.J. Fagan, C.M. Langton, Three dimensional stereolithography models of cancellous bone structures from μCT data: testing and validation of finite element results, Proc. Inst.Mech. Eng. H, 220, (2006), 481-484.

E.F. Donaldson, P. Pankaj, A.H. Law, A. H Simpson, Virtual trabecular bone models and their mechanical response, Proc. Inst. Mech. Eng. H, 222, (2008), 1185-1195.

X.N. Dong, X. E. Guo, The dependence of transversely isotropic elasticity of human femoral cortical bone on porosity, J. Biomech., 37, (2004), 1281-1287.

X.N. Dong, X.E. Guo, Prediction of cortical bone elastic constants by a two-level micromechanical model using a generalized self-consistent method, J. Biomech. Eng., 128, (2006), 309-316.

E.R.C. Draper, A.E. Goodship, A novel technique for four-point bending of small bone samples with semi-automatic analysis, J. Biomech., 36, (2003), 1497-1502.

D.K. Dubey, V. Tomar, Microstructure dependent dynamic fracture analyses of trabecular bone based on nascent bone atomistic simulations, Mech. Res. Comm., 35, (2008), 24-31.

A. Ekani-Nkodo, Size exclusion and diffusion of flouresceinated probes within collagen fibrils, Phys. Rev. E, 67, (2003), 021909-7.

G.M. Erickson, J. Catanese , T.M. Keaveny, Evolution of the biomechanical material properties of the femur, The Anatomical Record, 268, (2002), 115-

124.

D. Erts, L.J. Gathercole, E.D.T. Atkins, Scanning probe microscopy of intrafibrillar crystallites in calcified collagen, J. Mater. Sci. Mater. Med., 5, (1994), 200-206.

J.D. Eshelby, The determination of the elastic field of an ellipsoidal inclusion, and related problems, Proc. of the Royal Society of London Series A-Mathematical and Physical Sciences, 241, (1957), 376-396.

G.P. Evans, J.C. Behiri, J.D. Currey, W. Bonfield, Microhardness and Young modulus in cortical bone exhibiting a wide-range of mineral volume fractions, and in a bone analog, J. Mater. Sci. Mater. Med., 1, (1990), 38-43.

A.G. Evans, E.A. Charles, Fracture toughness determinations by indentation, J. Amer. Cer. Soc., 59, (1976), 371.

G.E. Fantner, T. Hassenkam, J.H. Kindt, J.C. Weaver, H. Birkedal, L. Pechenik, J.A. Cutroni, G. A.G. Cidade, G.D. Stucky, D.E. Morse, P.K. Hansma, Sacrificial bonds and hidden length dissipate energy as mineralized fibrils separate during bone fracture, Nat. Mater., 4, (2005), 612-616.

H. Follet, F. Peyrin, E. Vidal-Salle, A. Bonnassie, C. Rumelhart, P.J. Meunier, Intrinsic mechanical properties of trabecular calcaneus determined by finite-element models using 3D synchrotron microtomography, J.Biomech., 40(10), (2007), 2174-2183.

C.M. Ford, T.M. Keaveny, The dependence of shear failure properties of trabecular bone on apparent density and trabecular orientation, J. Biomech., 29, (1996), 1309-1317.

P. Fratzl, M. Groschner, G. Vogl, H. Plenk, J. Eschberger, N. Fratzl-Zelman, Mineral crystals in calcified tissues: A comparative study by SAXS, J. Bone Miner. Res., 7, (1992), 329-334.

P. Fratzl, N. Fratzl-Zelman, K. Klaushofer, Collagen packing and mineralization: An X-ray scattering investigation of turkey leg tendon, Biophys. J., 64, (1993), 260-266.

P. Fratzl, N. Fratzl-Zelman, K. Klaushofer, G. Vogl, K. Koller, Nucleation and growth of mineral crystals in bone studied by small- angle X-Ray scattering, Calcif. Tiss. Int., 48, (1991), 407–413.

A. Fritsch, C. Hellmich, 'Universal' microstructural patterns in cortical and trabecular, extracellular and extravascular bone materials: Micromechanics-

based prediction of anisotropic elasticity, J. Theor. Biol., 244, (2007), 597-620.

G.D. Fullerton, E. Nes, M. Amurao, A. Rahal, L. Krasnosselskaia, I. Cameron, An NMR method to characterize multiple water compartments on mammalian collagen, Cell Biol Intern, 30, (2006), 66-73.

G.D. Fullerton, M. Amurao, Evidence that collagen and tendon have monolayer water coverage in the native state, Cell Biol Intern, 30, (2006), 56-65.

H. Gao, B. Ji, I.L. Jager, E. Arzt, P. Fratzl, Materials become insensitive to flaws at nanoscale: Lessons from nature, PNAS, 100, (2003), 5597-5600.

J. Ghanbari, R. Naghdabadi, Nonlinear hierarchical multiscale modeling of cortical bone considering its nanoscale microstructure, J. Biomech., 42(10), (2009), 1560-1565.

L.J. Gibson, M.F. Ashby, B.A. Harley, Cellular Materials in Nature and Medicine, Cambridge University Press, Cambridge, UK, 2010.

L.J. Gibson, M.F. Ashby, G.S. Schajer, C.I. Robertson, The mechanics of two-dimensional cellular materials, Proc. R. Soc. Lond. A, 382, (1982), 25-42.

L.J. Gibson, M.F. Ashby, The mechanics of 3-dimensional cellular materials, Proc. R. Soc. Lond. A, 382, (1982), 43-59.

L.J. Gibson, The mechanical behaviour of cancellous bone, J. Biomech., 18, (1985), 317-328.

M.M. Giraud-Guille, Twisted plywood architecture of collagen fibrils in human compact bone osteons, Calcif. Tiss. Int., 42, (1988), 167-180.

M.J. Glimcher, Recent studies of the mineral phase in bone and its possible linkage to the organic matrix by protein-bound phosphate bonds, Philosophical Transactions of the Royal Society of London, 304, (1984), 479-508.

J. Goldstein, D.E. Newbury, D.C. Joy, C.E. Lyman, P. Echlin, E. Lifshin, L.Sawyer, J.R. Michael. Scanning Electron Microscopy and X-ray Microanalysis, Plenum Press. New York, 2003.

R.W. Goulet, S.A. Goldstein, M.J. Ciarelli, J.L. Kuhn, M.B. Brown, L.A. Feldkamp, The relationship between the structural and orthogonal compressive properties of trabecular bone, J. Biomech., 27, (1994), 375-377, 379-389.

Q. Grimal, G. Rus, W.J. Parnell, P. Laugier, A two-parameter model of the effective elastic tensor for cortical, J. Biomech., 44, (2011), 1621-1625.

Q. Grimal, S. Haupert, D. Mitton, L. Vastel, P. Laugier, Assesment of cortical bone elasticity and strength: Mechanical testing and ultrasound provide complementary data, Med. Eng. Phys., 31, (2009), 1140-1147.

E. Hamed, I. Jasiuk, Y. Lee, T. Liszka, Multiscale modeling of elastic moduli of trabecular bone, submitted, (2011).

E. Hamed, Y. Lee, I. Jasiuk. Multiscale modeling of elastic properties of cortical bone, Acta Mech., 213, (2010), 131-154.

U. Hansen, P. Zioupos, R. Simpson, The effect of strain rate on the mechanical properties of human cortical bone, J. Biomech. Eng., 130, (2008), 011011.

P. Hansma, P. Turner, B. Drake, E. Yurtsev, A. Proctor, P. Mathews, J. Lelujian, C.Randall, J. Adams, R. Jungmann, F. Garza-de-Leon, G. Fantner, H. Mkrtchyan, M. Pontin, A. Weaver, M. B. Brown, N. Sahar, R. Rossello, D. Kohn, The bone diagnostic instrument II: Indentation distance increase, Rev.Sci. Instrum., 79, (2008), 064303.

P. K. Hansma, P. J. Turner, G.E. Fantner, Bone diagnostic instrument, Rev. Sci. Instrum., 77, (2006), 075105.

N.M. Harrison, P.F. McDonnell, D.C. O'Mahoney, O.D. Kennedy, F.J. O'Brien, P.E. McHugh, Heterogeneous linear elastic trabecular bone modelling using micro-CT attenuation data and experimentally measured heterogeneous tissue properties. J. Biomech., 41, (2008), 2589-2596.

Z. Hashin, S.A. Shtrikman, A variational approach to the theory of the elastic behavior of multiphase materials J Mech Phys Solids, 11, (1963), 127-140.

T. Hassenkam, G.E. Fantner, J.A. Cutroni, J.C. Weaver, D.E. Morse, P.K. Hansma, High-resolution AFM imaging of intact and fracture trabecular bone, Bone, (2004), 35, 4-10.

C. Hellmich, J.F. Barthelemy, L. Dormieux, Mineral-collagen interactions in elasticity of bone ultrastructure - a continuum micromechanics approach, European Journal of Mechanics A-Solids, 23(5), (2004), 783-810.

C.J. Hernandez, G.S. Beaupre, T.S. Keller, D.R. Carter, The influence of bone volume fraction and ash fraction on bone strength and modulus, Bone, 29, (2001), 74-78.

A. Hershey, The elasticity of an isotropic aggregate of anisotropic cubic crystals, J. Appl. Mech. (ASME), 21, (1954), 236-240.

R. Hill, Elastic properties of reinforced solids- Some theoretical principles, Journal of the Mechanics and Physics of Solids, 11, (1963), 357-372.

R. Hill, Theory of mechanical properties of fiber-strengthened materials: I.Elastic behavior, J. Mech. Phys. Solids, 12, (1964) 199–212.

T.J. Hirsch, Modulus of elasticity of concrete affected by elastic moduli of cement paste matrix and aggregate, Proceedings of the American Concrete Institute, 59, (1962), 427-451.

T. Hoc, L. Henry, M. Verdier, D. Aubry, L. Sedel, A. Meunier, Effect of microstructure on the mechanical properties of Haversian cortical bone, Bone, 38, (2006), 466-474.

H.A. Hogan, Micromechanics modeling of haversian cortical bone properties, J. Biomech., 25, (1992), 549-556.

J. Homminga, B.R. Mccreadie, H. Weinans, R. Huiskes, The dependence of the elastic properties of osteoporotic cancellous bone on volume fraction and fabric, J. Biomech., 36(10), (2003), 1461-1467.

J. Homminga, R. Huiskes, B. Van Rietbergen, P. Rüegsegger, H. Weinans, Introduction and evaluation of a gray-value voxel conversion technique, J. Biomech., 34, (2001), 513–517.

K.D. Hunt, V.D. O'Loughlin, D.W. Fitting, L. Adler, Ultrasonic determination of the elastic modulus of human cortical bone, Med Biol. Eng. Comp., 36, (1998), 51-56.

S. Ilic, K. Hackl, K., R. Gilbert, Application of the multiscale FEM to the modeling of cancellous bone, Biomech. Model. Mechanobiol., 9, (2010), 87-102.

M. Ito, Assessment of bone quality using micro-computed tomography (micro-CT) and synchrotron micro-CT, J. Bone Miner. Metab., 23, (2005), 115-121.

M.J. Jaasma, H.H. Bayraktar, G.L. Niebur, T.M. Keaveny, Biomechanical effects of intraspecimen variations in tissue modulus for trabecular bone, J. Biomech., 35, (2002), 237-246.

S.A. Jackson, A.G. Cartwright, D. Lewis, The morphology of bone mineral crystals, Calcif. Tiss. Res., 25, (1978), 217-222.

I.L. Jager, P. Fratzl, Mineralized collagen fibrils: A mechanical model with a staggered arrangement of mineral particles, Biophys. J., 79, (2000), 1737-

1746.

I. Jasiuk, M. Ostoja-Starzewski, Modeling of bone at a single lamella level, Biomech. Model. Mechanobiol., 3, (2004), 67-74.

B. Ji, H. Gao, Elastic properties of nanocomposite structure of bone, Comp.Sci. Tech., 66, (2006), 1212–1218.

E.P. Katz, S. Li, Structure and function of bone collagen fibrils, J. Mol. Biol., 80, (1973), 1-15.

J.L. Katz, Anisotropy of Young's modulus of bone, Nature, 283, (1980), 106-107.

T. S. Keller, Predicting the compressive mechanical behavior of bone, J. Biomech., 27, (1994), 1159-1168.

T.S. Keller, Z. Mao, D.M. Spengler, Young modulus, bending strength, and tissue physical properties of human compact bone, J. Orthop. Res., 8, (1990), 592-603.

S.P. Kotha, N. Guzelsu, The effects of interphase and bonding on the elastic modulus of bone: changes with age-related osteoporosis, Med. Eng. Phys., 22, (2000), 575-585.

P. Kowalczyk, Elastic properties of cancellous bone derived from finite element models of parameterized microstructure cells, J. Biomech., 36, (2003), 961-972.

E. Kroner, Berechnung der elastichen konstanten des vielkristalls aus den konstanten des einkristalls, Zeitschrift Fur Physik, 151, (1958), 504-518.

R.M. Kulin, F.C. Jiang, K.S. Vecchio, J. Effects of age and loading rate on equine cortical bone failure, J. Mech. Behav. Biomed. Mater., 4, (2011), 57-75.

W.J. Landis, K.J. Hodgens, J. Arena, M.J. Song, B.F. McEwen, Structural relations between collagen and mineral in bone as determined by high voltage electron microscopic tomography, Microscopy Res. Tech., 33, (1996b), 192-202.

W.J. Landis, K.J. Hodgens, M.J. Song, J. Arena, S. Kiyonga, M. Marko, C. Owen, B.F. McEwen, Mineralization of collagen may occur on fibril surfaces: evidence from conventional and high-voltage microscopy and three-dimensional imaging, J. Struct. Biol., 117, (1996a), 24-35.

W.J. Landis, M.J. Song, A. Leigh, L. McEwen, B.F. McEwen, Mineral and

organic matrix interaction in normally calcifying tendon visualized in three dimensions by high-voltage electron microscopic tomography and graphic image reconstruction, J. Struct. Biol., 110, (1993), 39-54.

W.J. Landis, The strength of a calcified tissue depends in part on the molecular structure and organization of its constituent mineral crystals in their organic matrix, Bone, 16, (1995), 533-544.

M.D. Landrigan, J. Li, T.L. Turnbull, D.B. Burr, G.L. Niebur, R.K. Roeder, Contrast-enhanced micro-computed tomography of fatigue microdamage accumulation in human cortical bone, Bone, 48, (2011), 443–450.

M.E. Launey, M.J. Buehler, R.O. Ritchie, On the mechanistic origins of toughness in bone, Annu. Rev. Mater. Res., 40, (2010), 25-53.

J.L. Lewis, W. Goldsmith, The dynamic fracture and prefracture response of compact bone by split Hopkinson bar methods, J. Biomech., 8, (1975), 27-40.

C.T. Lim, E.H. Zhou, A. Li, S.R.K. Vedula, H.X. Fu, Experimental techniques for single cell and single molecule biomechanics, Mater. Sci. Eng. C, 26, (2006), 1278-1288.

F. Linde, P. Norgaard, I. Hvid, A. Odgaard, K. Soballe, Mechanical properties of trabecular bone – dependency on strain rate, J. Biomech., 24, (1991), 803-809.

S. Lohfeld, V. Barron, P.E. McHugh, Biomodels of bone: A review, Ann. Biomed. Eng., 33, (2005), 1295-1311.

A.C. Lorenzo, E.R. Caffarena, Elastic properties, Young's modulus determination and structural stability of the tropocollagen molecule: a computational study by steered molecular dynamics, J. Biomech., 38, (2005), 1527-1533.

J.C. Lotz, T.N. Gerhart, W.C. Hayes, Mechanical properties of trabecular bone from the proximal femur: a quantitative CT study, J. Comp. Ass. Tomography, 14, (1990), 107-114.

V.A. Lubarda, E. Novitskaya, J. McKittrick, S.G. Bodde, P.-Y. Chen, Elastic properties of cancellous bone in terms of elastic properties of its mineral and protein phases with application to their osteoporotic degradation, Mech.Mater., (2011), accepted.

G.L. Lucas, F.W. Cooke, E.A. Friis, A Primer on Biomechanics, Springer, New York, 1999.

J.K. Mackenzie, The elastic constants of solid containing spherical holes, Proc. Phys. Soc. Lond. B, 63, (1950), 2-11.

A.D. MacKerell, D. Bashford, M. Bellott, R.L. Dunbrack, J.D. Evanseck, M.J.Field, S. Fischer, J. Gao, H. Guo, S. Ha, D. Joseph-McCarthy, L. Kuchnir, K.Kuczera, F.T.K. Lau, C. Mattos, S. Michnick, T. Ngo, D.T. Nguyen, B.Prodhom, W.E. Reiher, B. Roux, M. Schlenkrich, J.C. Smith, R. Stote, J.Straub, M. Watanabe, J. Wiorkiewicz-Kuczera, D. Yin, M. Karplus, All-atom empirical potential for molecular modeling and dynamics studies of proteins, J. Phys. Chem. B, 102, (1998), 3586-3616.

R.B. Martin, D.B. Burr, N.A. Sharkey, Skeletal Tissue Mechanics, Springer Verlag, New York, 1998.

J.H. McElhaney, Dynamic response of bone and muscle tissue, J. Appl. Physiology, 21, (1966), 123.

J. McKittrick, P.-Y. Chen, L. Tombolato, E.E. Novitskaya, M.W. Trim, G.A. Hirata, E.A. Olevsky, M.F. Horstemeyer, M.A. Meyers, Energy absorbent natural materials and bioinspired design strategies: A review, Mater. Sci. Eng. C, 30, (2010), 331-342.

R. Müller, P. Ruegsegger, Three-dimensional finite element modelling of non-invasively assessed trabecular bone structures, Med. Eng. Phys., 17, (1995), 126- 133.

E.F. Morgan, O.C. Yen, W.C. Chang, T.M. Keaveny, Nonlinear behavior of trabecular bone at small strains, J. Biomed. Eng., 123, (2001), 1-9.

T. Mori, K. Tanaka, Average stress in matrix and average elastic energy of materials with misfitting inclusions, Acta Metallurgica, 21, (1973), 571-574.

R. Müller, M. Hahn, M. Vogel, G. Delling, P. Rüegsegger, Morphometric analysis of non-invasively assessed bone biopsies: comparison of high-resolution computed tomography and histologic sections, Bone, 18, (1996), 215–220.

R.K. Nalla, J.J. Kruzic , J.H. Kirmey, M. Ballooch, J.W. Ager, R.O. Ritchie, Role of microstructure in the aging-related deterioration of the toughness of human cortical bone, Mater. Sci. Eng.. C, 26, (2006), 1251-1260.

R.K. Nalla, M. Balooch, J.W. Ager, J.J. Kruzic, J.H. Kinney, R.O. Ritchie, Effects of polar solvents on the fracture resistance of dentin: role of water hydration, Acta Biomater. 1, (2005), 31-43.

S. Nemat-Nasser, M. Hori, Micromechanics: overall properties of heteroge-

neous Materials, Elsevier, Amsterdam, 1999.

S. Nemat-Nasser, T. Iwakuma, On composites with periodic structure Mechanics of Materials, Mech. .Mater., 1, (1982), 239-267.

S. Nikolov, D. Raabe, Hierarchical modeling of the elastic properties of bone at submicron scales: The role of extrafibrillar mineralization, Biophys. J., 94, (2008), 4220-4232.

P.M. Nolan, J. Peters, M. Strivens, D. Rogers, J. Hagan, N. Spurr, I.C. Gray, Vizor L., D. Brooker, E. Whitehill, A systematic, genome-wide, phenotype-driven mutagenesis programme for gene function studies in the mouse, Nat. Gen., 25, (2000), 440–443.

E.E. Novitskaya, P.-Y. Chen, S. Lee, A. Castro-Ceseña, G. Hirata, V.A. Lubarda, J. McKittrick, Anisotropy in the compressive mechanical properties of bovine cortical bone and the mineral and protein constituents, Acta Biomater., 7, (2011), 3170-3177.

F. J. O'Brien, D. Taylor, G.R. Dickson, T.C. Lee, Visualisation of three-dimensional microcracks in compact bone, J. Anat., 197, (2000), 413–420.

F. J. O'Brien, D. Taylor, T.C. Lee, An improved labeling technique for monitoring microcrack growth in compact bone, J. Biomech., (2002), 35, 523–526.

F. J. O'Brien, D. Taylor, T.C. Lee, Microcrack accumulation at different intervals during fatigue testing of compact bone J. Biomech., 36, (2003), 973–980.

A. Odgaard, Three-dimensional methods for quantification of cancellous bone architecture, Bone, 20, (1997), 315–328.

M.E. Oest, K.M. Dupont, H. Kong, D.J. Mooney, R.E. Guldberg, Quantitative assessment of scaffold and growth factor-mediated repair of critically sized bone defects, J. Orthop. Res., 25, (2007), 941-950.

W.C. Oliver, G.M. Pharr, Measurement of hardness and elastic modulus by instrumented nanoindentation: advances in understanding and refinements of the methodology, J. Mater. Res., 19, (2004), 3-20.

M.J. Olszta, X. Cheng, S.S. Jee, R. Kuman, Y-Y. Kim, M.J. Kaufman, E.P. Doublas, L.B. Gower, Bone structure and formation: A new perspective, Mater. Sci. Eng. R, 58, (2007), 77-116.

W.J. Parnell, Q. Grimal, The influence of mesoscale porosity on cortical bone anisotropy. Investigations via asymptotic homogenization, J. R. Soc. Interface,

6, (2009), 97-109.

R.M.V. Pidaparti, A. Chandran, Y. Takano, C.H. Turner, Bone minerals lies mainly outside collagen firbrils: predictions of a composite model for osteonal bone, J. Biomech., 29, (1996), 909-916.

K. Piekarski, Analysis of bone as a composite material, Int. J Eng Sci, 11, (1973), 557-565.

A. Postnov, A. Vinogradov, D. Van Dyck, S.V. Saveliev, N. M. De Clerck, Quantitative analysis of bone mineral content by x-ray microtomography, Physiol Meas., 24, (2003), 165–178.

K. Rajan, Linear elastic properties of trabecular bone - A cellular solid approach, J. Mater. Sci. Lett., 4, (1985), 609-611.

D.T. Reilly, A.H. Burnstein, The mechanical properties of cortical bone, J.Bone Joint. Surg. A, 56, (1974a), 1001-1022.

D.T. Reilly, A.H. Burstein, V.H. Frankel, The elastic modulus for bone, J. Biomech., 7, (1974b), 271-276.

A. Reuss, Berechnung der fliebgrenze von mischkristallen auf grund der plasticitatsbedingung fur einkristalle, ZAAM, 9, (1929), 49-58.

J.Y. Rho, M.E. II Roy, T.Y. Tsui, G.M. Pharr, Elastic properties of microstructural components of human bone tissue as measured by nanoindentation, J. Biomed. Mater. Res., 45, (1999), 48-54.

J.Y. Rho, J.D. Currey, P. Zioupos, G.M. Pharr, The anisotropic Young's modulus of equine secondary osteones and interstitial bone determined by nanoindentation, Journal of Experimental Biology, 204, (2001), 1775-1781.

J.Y. Rho, L. Kuhn-Spearing, P. Zioupos, Mechanical properties and the hierarchical structure of bone, Med. Eng. Phys., 20, (1998), 92-103.

J.Y. Rho, M.C. Hobatho, R.B. Ashman, Relations of mechanical properties to density and CT numbers in human bone, Med. Eng. Phys., 17, (1995), 347-355.

J.Y. Rho, R.B. Ashman, C.H. Turner, C. H., Young's modulus of trabecular and cortical bone material-ultrasonic and microtensile measurements, J. Biomech., (1993), 26, 111-119.

J.Y. Rho, T.Y. Tsui, G.M. Pharr, Elastic properties of human cortical and trabecular lamellar bone measured by nanoindentation, Biomater., 18, (1997),

1325-1330.

J.C. Rice, S.C. Cowin, J.A. Bowman, On the dependence of the elasticity and strength of cancellous bone on apparent density, J. Biomech., 21, (1988), 155-168.

B.L. Riggs, H.W. Wahner, W.L. Dunn, R.B. Bazess, K.P. Offord, L.J. Melton III, Differential changes in bone mineral densit of the appendicular and axial skeleton with aging, J. Clin. Invest., 67 (1981) 328-225.

R.O. Ritchie, M.J. Buehler, P. Hansma, Plasticity and toughness in bone, Phys Today, (2009), 41-47.

R.O. Ritchie, R.K. Nalla, J.W. Ager III, G. Balooch, J.H. Kinney, Fracture and ageing in bone: Toughness and structural characterization, Strain, 42, (2006), 225-232.

M.A. Rubin, I. Jasiuk, J. Taylor, J. Rubin, T. Ganey, R.P. Apkarian, TEM analysis of the nanostructure of normal and osteoporotic human trabecular bone, Bone, 33, (2003), 270-282.

O. Ruiz, R. Schouwenaars, E.I. Ramírez, V.H. Jacobo, A. Ortiz, Analysis of the architecture and mechanical properties of cancellous bone using 2D Voronoi cell based models, Proc. WCE I, (2010), 609-614.

S.D. Ryan, J.L. Williams, Tensile testing of rodlike trabeculae excised from bovine femoral bone, J. Biomech., 22, (1989), 351-355.

N. Sasaki, A. Tagami, T. Goto, M. Taniguchi, M. Nakata, K. Hikichi, Atomic force microscopic studies on the structure of bovine femoral cortical bone at the collagen fibril-mineral level, J. Mater. Sci. Mater. Med., 13, (2002), 333-337.

P. Schneider, M. Stauber, R. Voide, M. Stampanoni, L.R. Donahue, R. Müller, Ultrastructural properties in cortical bone vary greatly in two inbred strains of mice as assessed by synchrotron light based micro- and nano-CT, J. Bone Miner. Res., 22, (2007), 1557-1570.

E.D. Sedlin, C. Hirsch, Factors affecting the determination of the physical properties if femoral cortical bone, Acta Ortop. Scandinav., 37, (1966), 29-48.

T. Siegmund, M.R. Allen, D.B. Burr, Failure of mineralized collagen fibrils: Modeling the role of collagen cross-linking, J. Biomech., 41, (2008), 1427-1435.

M.J. Silva, L.J. Gibson, Modeling the mechanical behavior of vertebral trabec-

ular bone: effects of age-related changes in microstructure, Bone, 21, (1997), 191–199.

L.M. Siperko, W.J Landis, Aspects of mineral structure in normally calcifying avian tendon, J. Struct. Biol., 135, (2001), 313-320.

J.G. Skedros, J.I. Holmes, E.G. Vajda, R.D. Bloebaum. Cement lines of secondary osteons in human bone are not mineral-deficient: New data in a historical perspective, Anat. Rec. A, 286, (2006), 781-803.

S.R. Stock, MicroComputed tomography: methodology and applications, CRC Press, 2003.

C.T. Sun, S. Li, Three-dimensional effective elastic constants for thick laminates, J. Composite Mater., 22, (1988), 629-639.

K. Tai, M. Dao, S Suresh, A. Palazoglu, C. Ortiz, Nanoscale heterogeneity promotes energy dissipation in bone, Nature Mater., 6, (2007), 455-462.

K. Tanaka, Y. Kita, T. Katayama, M. Matsukawa, Mechanical properties of a single trabecula in bovine femur by the three point bending test, IFMBE Proceedings, 27, (2010), 235-238.

M. Taya, T.W. Chou, On two kinds of ellipsoidal inhomogeneities in an infinite elastic body: An application to a hybrid composite, Int. J. Solids Struct., 17, (1981), 553-563.

R.C. Tennyson, R. Ewert, V. Niranjan, Dynamic viscoelastic response of bone, Exper Mech, 12, (1972), 502-507.

P.J. Thurner, Atomic force microscopy and indentation force measurement of bone, WILEY Interdisciplinary reviews-nanomedicine and nanobiotechnology, 1, (2009), 624-649.

J.A. Timlin, A. Carden, M.D. Morris, Chemical microstructure of cortical bone probed by Raman transects, Appl. Spectrosc., 53, (1999), 1429-1435.

W. Tong, M.J. Glimcher, J.L. Katz, L. Kuhn, S.J. Eppell, Size and shape of mineralites in young bovine bone measured by atomic force microscopy, Calc.Tiss. Inter., 72, (2003), 592-598.

D. Toroian, J.L. Lim, P.A. Price, The size exclusion characteristics of type I collagen: implications for the role of non-collagenous bone constituents in mineralization, J. Biol. Chem., 282, (2007), 22437-22447.

S. Torquato, Effective stiffness tensor of composite media: II. Applications to

isotropic dispersions, J. Mech. Phys. Solids, 35, (1998), 1411–1440.

C.H. Turner, A. Chandran, R.M.V. Pidaparti, The anisotropy of osteonal bone and its ultrastruetural implications, Bone, 17, (1995), 85-89.

C.H. Turner, D.B. Burr, Basic biomechanical measurements of bone: a tutorial, Bone, 14, (1993), 595-608.

C.H. Turner, J. Rho, Y. Takano, T.Y. Tsui, G. M. Pharr, The elastic properties of trabecular and cortical bone tissues are similar: results from two microscopic measurement techniques, J. Biomech., 32, (1999), 437-441.

D. Ulrich, B. van Rietbergen, H. Weinans, P. Ruegsegger, Finite element analysis of trabecular bone structure: a comparison of image-based meshing techniques, J. Biomech., 31, (1998), 1187-1192.

D. Ulrich, T. Hildebrand, B. van Rietbergen, R. Muller, P. Ruegsegger, The quality of trabecular bone evaluated with micro-computed tomography, FEA and mechanical testing, Stud. Health Tech. Inform., 40, (1997) 97-112.

J.C. van der Linden, J.S. Day, J.A.N. Verhaar, H. Weinans, Altered tissue properties induce changes in cancellous bone architecture in aging and diseases, J. Biomech., 37, (2004), 367-374.

D.R. van der Rijt, D.W. van der Werf, M.L. Bennink, P.J. Dijkstra, J. Feijen, Micromechanical testing of individual collagen fibrils, Macromolec. Biosci., 6, (2006), 699-702.

A.C.T. van Duin, S. Dasgupta, F. Lorant, W.A. Goddard, ReaxFF: A reactive force field for hydrocarbons, J. of Phys. Chem. A, 105, (2001), 9396-9409.

T.M.G.J. van Eijden, L.J. van Ruijven, E.B.W. Giesen, Bone tissue stiffness in the andibular condyle is dependent on the direction and density of the cancellous structure, Calcif. Tiss. Int., 75, (2004), 502-508.

R.P. van Hove, P.A. Nolte, A.Vatsa, C.M. Semeins, P.L. Salmon, T.H. Smit, J.Klein-Nulend, Osteocyte morphology in human tibiae of different bone pathologies with different bone mineral density - Is there a role for mechanosensing? Bone, 45, (2009), 321–329.

G.H. van Lenthe, J.P.W. van den Bergh, A.R.M.M. Hermus, R. Huiskes, The prospects of estimating trabecular bone tissue properties from the combination of ultrasound, dual-energy X-ray absorptiometry, microcomputed tomography, and microfinite element analysis, J. Bone Miner. Res., 16, (2001), 550-555.

G.H. van Lenthe, M. Stauber, R. Muller, Specimen-specific beam models for fast and accurate prediction of human trabecular bone mechanical properties, Bone, 39, (2006), 1182-1189.

B. van Rietbergen, H. Weinans, R. Huiskes, A. Odgaard, A new method to determine trabecular bone elastic properties and loading using micromechanical finite-element models, J. Biomech., 28, (1995), 69-81.

P.J. Veld, M.J. Stevens, Simulation of the mechanical strength of a single collagen molecule, Biophys. J., 95, (2008), 33-39.

D. Voet, J.G. Voet, Biochemistry, John Wiley and Sons, 1995.

W. Voigt, Uber die beziehung zwischen den beiden elasticitats constantan isotroper korper, Ann. Phys. 38, (1889), 185-192.

J.H. Waarsing, J.S. Day, J.C. van der Linden, A.G. Ederveen, C. Spanjers, N.De Clerck, A. Sasov, J.A.N. Verhaar, H. Weinans, Detecting and tracking local changes in the tibiae of individual rats: a novel method to analyse longitudinal in vivo micro-CT data, Bone, 34, (2004), 163– 169.

N.J. Wachter, G.D. Krischak, M. Mentzel, M.R. Sarkar, T. Ebinger, L. Kinzl,L. Claes, P. Augat, Correlation of bone mineral density with strength and microstructural parameters of cortical bone in vitro, Bone, 31, (2002), 90–95.

L.J. Walpole, On bounds for the overall elastic moduli of inhomogeneous systems I, J Mech Phys Sol., 14, (1966a), 151–162

L.J. Walpole, On bounds for the overall elastic moduli of inhomogeneous systems II, J Mech Phys Sol., 14, (1966b), 289–301.

C. Wang, L. Feng, I. Jasiuk, Scale and boundary conditions effects on the apparent elastic moduli of trabecular bone modeled as a periodic cellular solid, J. Biomech. Eng., 131, (2009), 121008-121018.

E. Watchtel, S. Weiner, Small-angle X-ray scattering study of dispersed crystals from bone and tendon, J. Bone Miner. Res., 9, (1994), 1651-1655.

U.G.K. Wegst, M.F. Ashby, The mechanical efficiency of natural materials, Phil. Mag., 21, (2004), 2167-2181.

S. Weiner, H.D. Wagner, The material bone: Structure mechanical function relations, Ann. Rev. Mater. Sci., 28, (1998), 271-298.

S. Weiner, P.A. Price, Disaggregation of bone into crystals, Calcif. Tiss. Int., 39, (1986a), 365-375.

S. Weiner, T. Arad, I. Sabanay, W. Traub, Rotated plywood structure of primary lamellar bone in the rat: Orientations of the collagen fibril arrays, Bone, 20, (1997), 509-514.

S. Weiner, W. Traub, Bone structure: From angstroms to microns, FASEB J., 6, (1992), 879-885.

S. Weiner, W. Traub, H.D. Wagner, Lamellar bone: structure – function relations, J. Struct. Biol., 126, (1986b), 241-255.

L. Yang, K.O. Van Der Werf, B.F. Koopman, V. Subramaniam, M.L. Bennink, P.J. Dijkstra, J. Feijen, Micromechanical bending of single collagen fibrils using atomic force microscopy, J. Biomed. Mater. Research A, 82A, (2007), 160-168.

A. Yoo, I. Jasiuk, Couple-stress moduli of a trabecular bone idealized as a 3D periodic cellular network, J. Biomech., 39, (2006), 2241-2252.

Y.J. Yoon, S.C. Cowin, The estimated elastic constants for a single bone osteonal lamella, Biomech. Model. Mechanobiol., 7, (2008), 1-11.

F. Yuan, S.R. Stock, D.R. Haeffner, J.D. Almer, D.C. Dunand, L.C. Brinson, A new model to simulate the elastic properties of mineralized collagen fibril, Biomech. Model. Mechanobiol., 10, (2011),147–160.

D. Zhang, D.D. Arola, J.A. Rouland, Evaluating the elastic modulus of bone using electronic speckle pattern interferometry, Exp. Tech., 25, (2001), 32-34.

M.C. Zimmerman, A. Prabhakar, B.V. Chokshi, N. Budhwani, H. Berndt, The acoustic properties of normal and imbedded bovine bone as measured by acoustic microscopy, J. Biomed. Mater. Res., 28, (1994), 931-938.

P. Zioupos, J.D. Currey, A. Casinos, Exploring the effects of hypermineralisation in bone tissue by using an extreme biological example, Connect. Tiss. Res., 41, (2000), 229-248.

P. Zioupos, U. Hansen, J.D. Currey, Microcracking damage and the fracture process in relation to strain rate in human cortical bone tensile failure, J. Biomech., 41, (2008), 2932-2939.

V. Ziv, S. Weiner, Bone crystal sizes: A comparison of transmission electron microscopic and X-ray diffraction width broadening techniques, Connect. Tiss. Res., 30, (1994), 165-175.

P.K. Zysset, Indentation of bone tissue: a short review, Osteoporos. Int., 20, (2009), 1049-1055.

P.K. Zysset, X.E. Guo, C.E. Hoffler, K.E. Moore, S.A. Goldstein, Elastic modulus and hardness of cortical and trabecular bone lamellae measured by nanoindentation in the human femur, J. Biomech., 32, (1999), 1005-1012.

P.K. Zysset, X.E. Guo, C.E. Hoffler, K.E. Moore, S.A. Goldstein, Mechanical properties of human trabecular bone lamellae quantified by nanoindentation, Technol. Health Care, 6, (1998), 429-432.

Submitted on January 2011.

Savremena dostignuća u mjerenju i sračunavanju modula elastičnosti kortikalnih i trabekularnih kostiju: kritički osvrt

U radu su prikazana savremena dostignuća u mjerenju i sračunavanju elastičnih svojstava kortikalnih i trabekularnih kostiju. Kost je multifunkcionalan materijal koji, izmedju ostalih funkcija, obezbedjuje oslonac ostalim tkivima u organizmu. Kao strukturalni materijal, kost se odlikuje čvrstinom, jačinom, žilavoscu, malom specifičnom težinom i prilagodljivošću. Njena izuzetna mehanička svojstva su posljedica njene složene, kompozitne i hijerarhijske strukture. U radu je dat kritički osvrt na eksperimentalne pristupe i metode koji se danas koriste za karakterizaciju sastava i strukture kostiju na nekoliko hijerarhijskih nivoa. Zatim su navedeni i diskutovani različiti analitički i računski metodi za odredjivanje elastičnih svojstava kostiju. Na kraju je ukazano na niz otvorenih i izazovnih problema u ovoj aktuelnoj oblasti biomehanike. Izloženi rezultati mogu biti od interesa u ortopediji i u sintezi novih bio-inspirisanih kompozitnih materijala za upotrebu u različitim oblastima inženjerstva.

doi:10.2298/TAM1103209N Math.Subj.Class.: 74A60, 74Q15, 74L15, 74M25.